Unique Ligand Selectivity of the GPR92/LPA$_5$ Lysophosphatidate Receptor Indicates Role in Human Platelet Activation[*][S]

Jesica R. Williams[‡], Anna L. Khandoga[§], Pankaj Goyal[§], James I. Fells[‡], Donna H. Perygin[‡], Wolfgang Siess[§], Abby L. Parrill[‡], Gabor Tigyi[¶], and Yuko Fujiwara[¶][1]

From the [‡]Department of Chemistry and Computational Research on Materials Institute, University of Memphis, Memphis, Tennessee 38152, the [§]Institute for Prevention of Cardiovascular Diseases, Medical Faculty, University of Munich, 80336 Munich, Germany, and the [¶]Department of Physiology, University of Tennessee Health Science Center, Memphis, Tennessee 38163

Lysophosphatidic acid (LPA) is a ligand for LPA$_{1-3}$ of the endothelial differentiation gene family G-protein-coupled receptors, and LPA$_{4-8}$ is related to the purinergic family G-protein-coupled receptor. Because the structure-activity relationship (SAR) of GPR92/LPA$_5$ is limited and whether LPA is its preferred endogenous ligand has been questioned in the literature, in this study we applied a combination of computational and experimental site-directed mutagenesis of LPA$_5$ residues predicted to interact with the headgroup of LPA. Four residues involved in ligand recognition in LPA$_5$ were identified as follows: R2.60N mutant abolished receptor activation, whereas H4.64E, R6.62A, and R7.32A greatly reduced receptor activation. We also investigated the SAR of LPA$_5$ using LPA analogs and other non-lysophospholipid ligands. SAR revealed that the rank order of agonists is alkyl glycerol phosphate > LPA > farnesyl phosphates ≫ N-arachidonoylglycine. These results confirm LPA$_5$ to be a *bona fide* lysophospholipid receptor. We also evaluated several compounds with previously established selectivity for the endothelial differentiation gene receptors and found several that are LPA$_5$ agonists. A pharmacophore model of LPA$_5$ binding requirements was developed for *in silico* screening, which identified two non-lipid LPA$_5$ antagonists. Because LPA$_5$ transcripts are abundant in human platelets, we tested its antagonists on platelet activation and found that these non-lipid LPA$_5$ antagonists inhibit platelet activation. The present results suggest that selective inhibition of LPA$_5$ may provide a basis for future anti-thrombotic therapies.

Lysophosphatidic acid (LPA,[2] 1-radyl-2-hydroxy-*sn*-3-glycero phosphate) specifically interacts with several protein tar-

gets that regulate physiological and pathophysiological processes (1–3). LPA targets include specific G-protein-coupled receptors (GPCRs) that mediate a wide variety of biological effects, including cell proliferation (4), cell survival (5), cell migration (6), and platelet aggregation (7, 8). GPCRs are the largest family of transmembrane receptors and represent targets of many therapeutics (9). Eight LPA-specific mammalian GPCRs, LPA$_{1-8}$, have been identified to date (10–12). Among the eight LPA receptors, LPA$_1$, LPA$_2$, and LPA$_3$ are members of the endothelial differentiation gene (EDG) family (13), and the transmembrane domains of human LPA$_{1-3}$ show 81% homology with each other (14). The five other members of the EDG family are specific for the related lysophospholipid sphingosine 1-phosphate (S1P). The structural foundation for LPA selectivity over S1P has been linked to a single amino acid at position 3.29, a conserved glutamine in the LPA-specific and glutamate in the S1P-specific members of the EDG family (14–16). However, the recently identified non-EDG family LPA receptors, LPA$_4$/p2y9 (13), LPA$_5$/GPR92 (17, 18), LPA$_6$/GPR87 (19), LPA$_7$/p2y5 (12), and LPA$_8$/p2y10 (10), are more closely related to the purinoreceptor gene cluster and share less than 20% amino acid identity with EDG-LPA receptors. Although EDG-LPA receptors have been well characterized and differences in ligand selectivity among LPA$_{1-3}$ have been reported (20, 21), the SAR of LPA$_5$ is presently limited to only a few LPA species (17, 18, 22). Further complicating this issue is a recent report by Oh da *et al.* (22) that suggests that two other naturally occurring ligands, farnesyl pyrophosphate (FPP) and *N*-arachidonoylglycine (NAG), are more potent agonists for LPA$_5$/GPR92 than LPA 18:1, which necessitates a re-classification of LPA$_5$ not as an LPA receptor.

We have previously generated computational models of each EDG-LPA receptor (14, 16, 21, 23), validated the models with site-directed mutagenesis, identified residues involved in ligand-induced activation of the receptors, and developed pharmacophore models enabling the *in silico* identification of selective ligands. However, LPA$_{4-8}$ exhibit little sequence identity

with LPA$_{1-3}$, and thus we hypothesized that these receptors may have unique properties and recognize LPA by different motifs as well as display SAR distinct from LPA$_{1-3}$. The investigation of the P2Y family of LPA GPCR represents a unique opportunity to examine how nature "developed" specific recognition of the same ligand using two significantly different primary sequences on the seven-transmembrane receptor template.

LPA contained in mildly oxidized low density lipoprotein and the lipid-rich core of atherosclerotic plaque elicit platelet activation (3, 9, 24). The receptor(s) mediating LPA-induced platelet activation is/are unknown. Several previous observations suggest that LPA$_5$ might be responsible for the currently unexplained effects of LPA on platelets. LPA$_5$ couples to G$_{12/13}$-mediated Rho activation and G$_q$-mediated phospholipase C activation. Similarly in platelets, LPA stimulates Rho and Ca^{2+} mobilization; low LPA concentrations induce Rho/Rho kinase-mediated shape change, and higher LPA concentrations stimulate an increase of cytosolic Ca^{2+} and aggregation (25–28). LPA$_5$ can also mediate an increase in intracellular cAMP production independent of G$_s$ (18), and cAMP formation inhibits platelet activation, which implies that LPA$_5$ activation could inhibit platelet aggregation. At the same time, a decrease in cAMP is insufficient to produce full platelet activation, suggesting other signaling events are needed for full platelet activation (29). LPA$_5$ receptor mRNA is one of the most abundant LPA GPCR mRNAs in human platelets (28, 30). Recently, we found that heterologously expressed LPA$_5$ showed similar SAR to that of platelets with preference to alkyl-glycerophosphate (AGP, also known as alkyl-LPA) over acyl-LPA (28). However, there are also discrepancies. Whereas albumin inhibits LPA-induced platelet activation, this effect is not observed in LPA$_5$-transfected cells (28), and LPA does not elevate cAMP levels in platelets, which is observed in LPA$_5$-transfected cells (18). These findings argue against the involvement of LPA$_5$ in platelet activation. Therefore, a comprehensive characterization of the LPA$_5$ receptor could help define the receptor responsible for mediating LPA effects on platelets.

In this study, the residues involved in ligand recognition by LPA$_5$ were identified using a combination of computational and experimental mutagenesis methods. Three cationic residues (Arg-2.60, Arg-6.62, and Arg-7.32) in TM segments 2, 6, and 7 are critical for ligand recognition of LPA$_5$, whereas two cationic residues (Arg-3.28 and Lys-7.35 (or Arg-7.36)) and a neutral polar residue (Gln-3.29) in TM segments 3 and 7 are required for EDG family LPA receptors. These results represent fundamental differences in ligand recognition between EDG and purinergic LPA receptors.

We also investigated the SAR of LPA$_5$ using LPA analogs with various chain lengths and degrees of unsaturation and other non-lysophospholipid ligands to determine whether this receptor can be classified as an LPA receptor based on the rank order of its naturally occurring agonists. Our data show that LPA, AGP, and cyclic phosphatidic acid (CPA) analogs in addition to farnesyl monophosphate (FMP) and FPP are ligands of LPA$_5$. We found LPA18:1 to be a more potent ligand of LPA$_5$ than farnesyl phosphate analogs (EC$_{50}$ = 8.9 ± 0.7 for LPA 18:1;

40 ± 15 for FPP; 49 ± 13 for FMP), thus confirming LPA$_5$/GPR92 to be a member of the non-EDG LPA receptor family.

Based on the SAR, we developed a receptor-based pharmacophore model of LPA$_5$ and applied it to *in silico* screening using the NCI data base browser and subsequent similarity searching in the Hit2Lead data base. Fifteen candidate compounds were tested, and two novel non-lipid LPA$_5$ antagonists were identified.

Finally, we investigated the involvement of LPA$_5$ in human platelet activation by testing the LPA$_5$ agonists and antagonists we identified in this study. Octadecenyl phosphate, an LPA$_4$ and LPA$_5$ agonist, induced platelet shape change as potently as AGP 18:1. FPP and FMP (antagonists of LPA$_{2,3,4}$ and potent LPA$_5$ agonists) and carba-CPA (CCPA, LPA$_5$-selective agonist) also induced platelet shape change. On the other hand, the two LPA$_5$ antagonists identified by *in silico* screening inhibited LPA-induced platelet shape change. Together, these data suggest LPA$_5$ is involved in human platelet activation.

EXPERIMENTAL PROCEDURES

Reagents—With the exception of polyunsaturated species of LPA, CPA and AGP analogs were purchased from Avanti Polar Lipids (Alabaster, AL). Polyunsaturated LPA species were obtained from Echelon Bioscience, Inc. (Salt Lake City, UT). FMP and FPP were purchased from Sigma. NAG was purchased from Cayman Chemical (Ann Arbor, MI). CCPA 16:1 and 18:1 were provided by Dr. Susumu Kobayashi (University of Tokyo, Tokyo, Japan) (31). Accurate concentrations of phospholipids were measured by phosphate assays (32), and lipids were prepared before use as 1 mM stocks in PBS containing 1 mM charcoal-stripped bovine serum albumin (BSA). BSA (fraction V, fatty acid-free) and anti-FLAG M2 monoclonal antibody were purchased from Sigma. Dulbecco's modified Eagle's medium was from Cellgro (Herndon, VA). Alexa Fluor 488-conjugated donkey anti-mouse IgG was purchased from Molecular Probes (Eugene, OR), and Fura-2 AM was from Invitrogen.

Residue Nomenclature—Amino acids in the TM domains were assigned index positions to facilitate comparison between GPCR with different numbers of amino acids, as described by Ballesteros and Weinstein (33). An index position is in the format *X.YY*. *X* denotes the TM domain in which the residue appears. *YY* indicates the position of that residue relative to the most highly conserved residue in that TM domain, which is arbitrarily assigned position 50.

Computational Model Development and Refinement—A homology model of the LPA$_5$ receptor was built based on a previously published LPA$_1$ receptor model (14, 16, 21, 23) with the Molecular Modeling Environment (MOE) software program using the sequence alignment shown in Fig. 1. The resulting model was geometry-optimized using the MMFF94 forcefield (34) to a root mean square gradient (RMSG) of 0.1 kcal/mol·Å. A multifragment search (MOE, version 2004, Chemical Computing Group, Montreal, Canada) was performed in MOE to randomly place methyl phosphate fragments within the receptor ([supplemental Fig. 1](#)). Fragment positions were optimized relative to the receptor to identify favorable phosphate interaction sites. The model was refined by examination of the conformational flexibility of more distant arginines. AGP 18:1
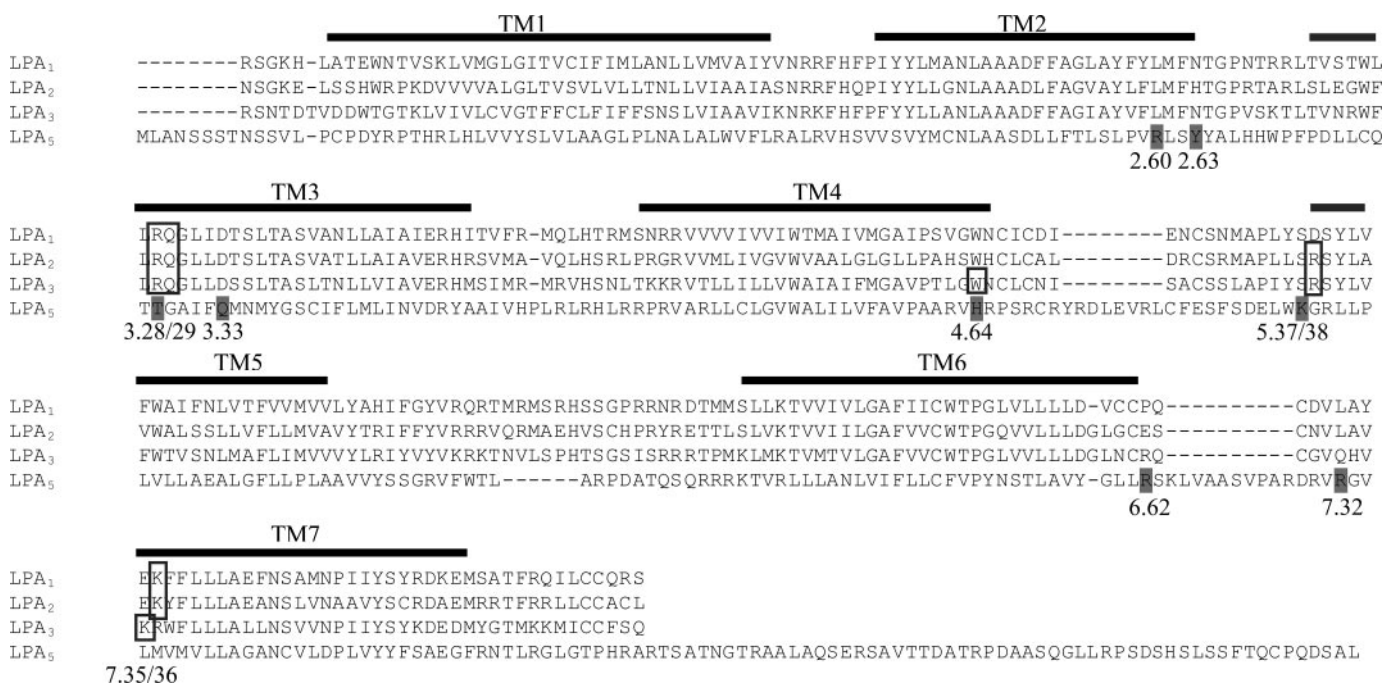
FIGURE 1. **Sequence alignments of EDG family of LPA receptors (LPA$_1$, LPA$_2$, and LPA$_3$) and LPA$_5$.** *Dark gray highlights* indicate positions mutated in this study. Residues with *black boxes* were mutated in other reports and are identified as important residues affecting ligand recognition.

was manually positioned inside the binding pocket of the receptor model based on the optimal methyl phosphate position from the multifragment search, and the side chains of Arg-2.60 and Arg-7.32 were rotated inward toward the phosphate headgroup of the ligand to permit optimal ligand-receptor electrostatic interactions. The modified receptor model was geometry-optimized using the MMFF94 forcefield (34) to a 0.1 kcal/mol·Å RMSG. The model was further refined by extending the helical segments of TM6 and TM7 to more accurately match the mutagenesis data. The helical segments of TM6 and TM7 were extended toward the extracellular space by replacing the structure of residues Leu-6.60 to Val-6.66 and Arg-7.30 to Met-7.36, respectively, with ideal helical segments. Extracellular loop 3 of the refined receptor model was geometry-optimized to an RMSG of 0.1 kcal/mol·Å followed by unrestrained optimization of the entire receptor to an RMSG of 0.1 kcal/mol·Å. The model was finalized by restraining the distances between the phosphate headgroup of LPA 18:1 and Arg-2.60, Arg-6.62, Arg-7.32. The ligand-receptor complex was minimized with the MMFF94 forcefield (34) with the distance-dependent dielectric constant set at 1. The final receptor model was geometry-optimized to a RMSG of 0.1 kcal/mol·Å.

Ligand Docking—Following model refinement AGP, LPA, CPA, 2CCPA, and 3CCPA, ligands were docked into the final receptor model with AutoDock 4.0 (35) as in our previous studies (21). Acyl and alkyl chain phosphate headgroups were docked into the model with a −2 charge. Cyclic phosphate headgroups were docked into the model with a −1 charge. Default docking parameters were used except for number of runs (15), energy evaluations (9.0×10^{10}), generations (30,000), and local search iterations (3000) with a docking box of 65 × 50 × 95 grid points and grid spacing of 0.375 Å. The receptor grid was centered near Arg-2.60. The docking box contained

the lower half of the extracellular domain and upper two-thirds of the transmembrane domains of the final receptor model. The docked conformations of the ligands were analyzed for key electrostatic interactions with the mutated residues.

Site-directed Mutagenesis—LPA$_5$ was mutated at residues computationally predicted to participate in ligand interactions as well as at residues corresponding to those with validated involvement in ligand recognition of EDG family LPA receptors using either the PCR-based overlap extension method or the QuikChange II XL site-directed mutagenesis kit (Stratagene, La Jolla, CA). TOP10 competent cells (Invitrogen) were transformed with the mutant constructs, and clones were verified by complete sequencing of the inserts. The list of mutants is in Table 1.

Measurement of Intracellular Ca^{2+} Mobilization—McArtl hepatoma RH7777 cells (ATCC) were plated in 60-mm dishes at a density of 0.8×10^6. After overnight incubation, the cells were transfected with 1 μg of plasmid DNA with Effectene (Qiagen, Valencia, CA), according to the manufacturer's instructions for 24 h, then re-plated onto poly-L-lysine-coated 96-well plates at a density of 5×10^4 cells/well, and cultured overnight. The following day, the culture medium was replaced with modified Krebs buffer, and the cells were serum-starved for 4 h. Subsequently, cells were loaded with Fura-2 AM for 30 min in modified Krebs buffer containing 2% (v/v) pluronic acid. After incubating the cells with Fura-2 AM, the cells were rinsed with Krebs buffer, and changes in the intracellular Ca^{2+} concentration were monitored by determining the ratio of emitted light intensities at 520 nm in response to excitation at 340 and 380 nm using FLEXstation II (Molecular Devices, Sunnyvale, CA). Each well was monitored for 80 s. The test compounds were added automatically after 15 s of base-line measurement.

Flow Cytometric Analysis—Cell surface expression of LPA$_5$ and its mutants was confirmed by flow cytometric analysis using immunofluorescence staining with anti-FLAG M2 monoclonal antibody. RH7777 cells were transfected with FLAG epitope-tagged LPA receptor constructs and cultured for 24 h. The culture medium was replaced with serum-free medium for 4 h before collection. The cells were detached using HyQTase Cell Detachment Solution (Hyclone Laboratories, Logan, UT), collected on ice, washed once with wash buffer (PBS, pH 7.4, containing 3% BSA), and incubated for 30 min in the buffer containing 5% normal donkey serum. The cells were incubated with anti-FLAG M2 monoclonal antibody (1:200) in 5% BSA/PBS for 1 h, followed by two washes, and then incubated with Alexa Fluor 488-conjugated donkey anti-mouse (1:1600) in PBS containing 5% BSA for 30 min. Cells were analyzed using an LSR II flow cytometer (BD Biosciences), and data were analyzed using CellQuest software (BD Biosciences) and FlowJo software (TreeStar Inc, Ashland, OR).

cAMP-response Element (CRE)-Luciferase Reporter Gene Assay—RH7777 cells were transiently transfected with pCRE-Luc plasmid DNA (Stratagene) and either LPA$_5$ wild type (WT) or its mutants using Effectene (Qiagen). Twenty four hours following transfection, cells were plated onto 96-well microplates at 3×10^4 cells/well. Twelve hours later, the culture medium was changed to serum-free medium for overnight. The following day, either vehicle, 10 μM LPA, or 50 μM forskolin was added to the cells for 3 h. Subsequently, One-Glo^{TM} luciferase assay reagent (Promega, Madison, WI) was added to the cells, and after 10 min of incubation at room temperature, luminescence responses were measured by Fusion α-plate reader (PerkinElmer Life Sciences). Luciferase activity was calculated as a percentage of the LPA-induced luminescence response in WT LPA$_5$-transfected cells.

Modeling of Receptor Mutants—The LPA 18:1 complex with LPA$_5$ was used to generate the four models of mutants L5.41N, L5.45N, L7.35N, and V7.39N by side chain replacements. Each mutant model was geometry-optimized with the MMFF94 forcefield and subjected to molecular dynamics to allow surrounding amino acid side chain positions to adapt to the substitution as we have done in previous studies (14, 36). Simulations were performed using the NVT ensemble (with temperature, volume, and number of molecules held constant) and the Nosé-Poincaré-Anderson (37) equations of motion. Kinetic energy was added to the system during a 30-ps heat phase during which the temperature was smoothly scaled from 0 to 300 K. The production phase was performed at a constant 300 K temperature for 100 ps. A time step of 2 fs was utilized with constrained bond lengths to hydrogen atoms. Following molecular dynamics, the structure obtained at 100 ps was geometry-optimized using the MMFF94 forcefield. LPA was removed and docked back into the mutant models using Autodock 4.0.

Pharmacophore Modeling—Common features of AGP 18:1, AGP 16:0, LPA 18:1, LPA 18:3, and CPA 18:1 docked in common regions within the receptor model were used to develop the three-point receptor-based pharmacophore. The pharmacophore points consisted of an anionic region, a hydrogen bond donor/acceptor region, and a hydrophobic region. The distances between these three regions were measured for the flexibly docked conformation of the most potent agonist AGP 18:1. The docked conformations of AGP 16:0, LPA 18:1, LPA 18:3, and CPA 18:1 were used to define appropriate radii for the pharmacophore points. The distance ranges defined by the maximum and minimum distances between spheres were used to search the NCI data base. The majority of hits obtained from this search were symmetric with acidic functional groups at both ends, unlike the known agonists. An asymmetric monoanionic analog of the hit NSC55155 (monoethyl ester) was utilized as a similarity search target with a 70% threshold in the Hit2Lead data base to identify leads for screening. The candidates were docked into the LPA$_5$ receptor model and prioritized for experimental screening based on the distances between their anionic headgroup and the critical residues Arg-2.60, Arg-7.32, and His-4.64. A final set of 14 compounds from this similarity search was selected to determine the required shape for LPA$_5$ receptor interaction.

Isolation of Platelets and Measurement of Platelet Shape Change—For measurement of shape change, human platelets were treated with acetylsalicylic acid and isolated in the presence of apyrase as described previously (38). Platelets were resuspended at a concentration of $4 \times 10^5/\mu$l in buffer C (20 mM Hepes, 138 mM NaCl, 2.9 mM KCl, 1 mM MgCl$_2$, 0.36 mM NaH$_2$PO$_4$, 5 mN glucose, 0.6 unit of ADPase/ml apyrase, pH 7.4). The compounds were dissolved (generally at 5 mM concentration) in methanol (2CCPA 16:1, 3CCPA 16:1, octadecenyl phosphate), ethanol (LPA, AGP, and NAG), or DMSO (octyl thiophosphatidic acid, H2L 5987411, and H2L 5765834) and stored at -80 °C. The solvents at the highest concentration tested (0.25% v/v) had no effect on platelet activation. Suspensions of washed platelets were transferred into aggregometer cuvettes, incubated at 37 °C, and exposed to various concentrations of the substances or vehicle control. Shape change was measured by the decrease in light transmission of the stirred (1100 rpm) platelet suspension in a LABOR aggregometer (Fresenius, Bad Homburg, Germany).

RESULTS

Selection of Mutation Sites—To investigate residues that interact with the phosphate headgroup of the ligands, we built a homology model of LPA$_5$ receptor based on a previously published LPA$_1$ receptor model (14, 16, 21, 23). We chose the LPA$_1$ model as a starting point because none of the GPCR for which crystal structures are available provides a higher degree of sequence homology. We have previously extensively evaluated the ligand recognition of LPA$_{1-3}$ and the S1P receptors, S1P$_1$ and S1P$_4$, using computational model-guided mutagenesis (14, 16, 21, 39, 40), and we have identified a cluster of four nearly conserved amino acid residues critical for ligand-induced receptor activation. The residue at 3.28 is a positively charged arginine residue in all the EDG family of S1P and LPA receptors, and the adjacent residue at 3.29 is glutamic acid in all EDG-S1P receptors and glutamine in all EDG-LPA receptors. A positively charged residue in TM7 is nearly conserved in all EDG family receptors. These results directed us to investigate positively charged residues in the LPA$_5$ receptor. Based on the aligned LPA$_{1-7}$ receptor sequences and the initial LPA$_5$ com-

Ligand Selectivity and Role in Platelet Activation of LPA$_5$

TABLE 1

Cell surface expression of WT and LPA$_5$ mutant receptors determined by flow cytometry using anti-FLAG antibody staining in transiently transfected RH7777 cells

Receptor constructs	Anti-FLAG-stained cells (% total cells)
pcDNA3.1 vector	<3.0
Wild type	24.3–49.0 ($n = 9$)
R2.60A	1.5
R2.60N	22.5
Y2.63A	65.1
T3.28A	63.1
Q3.33A	66.9
H4.64A	24.0
H4.64Q	61.7
K5.37A	35.5
R6.62A	50.1
R7.32A	42.8
R6.62A/R7.32A	48.2
L5.41N	32.1
L5.45N	3.27
L7.35N	33.4
V7.39N	36.1

putational model, we selected three positively charged residues, Arg-2.60, Arg-6.62, and Arg-7.32, which are conserved in at least three of the LPA$_{4-8}$ receptors, to assess the interaction with the phosphate headgroup of LPA. Furthermore, the multifragment search performed on the preliminary receptor model predicted these as well as four additional amino acids positioned less than 4.5 Å from the headgroup of LPA. Tyr-2.63 and Thr-3.28 were predicted to hydrogen bond to the phosphate group, and Gln-3.33 and His-4.64 were predicted to hydrogen bond to the hydroxyl group of LPA (supplemental Fig. 1). Thus, the sequence alignment and the multifragment search led us to hypothesize that replacement of these residues would have impact on receptor activation by LPA.

Characterization of the Cell Surface Expression of the Receptor Mutants—To validate and refine our computational model of the polar headgroup interactions, we generated site-directed mutants of the N-terminally FLAG epitope-tagged LPA$_5$ receptor construct. Cell surface expression of the receptor constructs was verified by flow cytometric analysis using FLAG-M2 antibody against the N-terminal FLAG epitope (Table 1). All receptor constructs were expressed on the cell surface when transiently transfected into RH7777 cells, except for the R2.60A mutant, which was not expressed at a detectable level. However, the asparagine mutant R2.60N showed cell surface expression and was used for further experiments. Variation in cell surface expression level occurred between some mutant receptors and the WT receptor. However, we have previously examined the impact of LPA receptor cell surface expression levels on potency (EC$_{50}$) and efficacy (E_{max}), and we demonstrated that differences in expression level over a wide range have no effect on ligand potency (14). Thus, the variations found are unlikely to impact the pharmacological properties of these mutants.

Effects of Mutations on LPA-induced Ca^{2+} Mobilization—We evaluated the impact of each mutation on the EC$_{50}$ and E_{max} of LPA 18:1-induced intracellular Ca^{2+} mobilization in transiently transfected RH7777 cells. The alanine mutations at Thr-3.28, Tyr-2.63, and Gln-3.33 showed EC$_{50}$ values of 21 $\pm$ 8.6, 69 $\pm$ 22, and 47 $\pm$ 24 nM, respectively. These potencies are comparable with the 16 $\pm$ 3.0 nM EC$_{50}$ of the WT (Fig. 2A),

suggesting that none of these residues have critical interactions with the polar headgroup of LPA. Maximal activation of the Y2.63A and Q3.33A mutants was higher than that of WT (122 $\pm$ 7.0 and 133 $\pm$ 6.4% of WT E_{max}, respectively); however, as we observed in our previous study (14), surface expression levels may alter the efficacy but not the potency of ligand-induced receptor activation. For this reason, the increase of E_{max} observed with Y2.63A and Q3.33A mutants could reflect the higher expression levels of these mutants than that of WT (Table 1). In contrast to T3.28A, Y2.63A, and Q3.33A, the R2.60N mutant showed no activation, suggesting that this residue is required (Fig. 2B). Alanine replacement at Arg-6.62 shifted the EC$_{50}$ from 16 $\pm$ 3.0 to 191 $\pm$ 25 nM, while retaining the WT-like E_{max} (Fig. 2B). In contrast, the replacement of Arg-7.32 with alanine diminished maximal activation by LPA, while also causing >45-fold increase in EC$_{50}$ (Fig. 2B). The >10-fold shift in EC$_{50}$ with R6.62A and R7.32A mutants led us to hypothesize that double mutations at Arg-6.62 and Arg-7.32 may eliminate the activation of the receptor by LPA. As shown in Fig. 2B, the R6.62A/R7.32A double mutant showed no activation by LPA. These data suggest both Arg-6.62 and Arg-7.32 are involved in the recognition of LPA, and that at least one is essential. Replacement of histidine at 4.64 with alanine showed 20-fold increase in EC$_{50}$, suggesting that this residue might interact with the phosphate group of LPA (Fig. 2C). Histidine can be protonated at one or both nitrogen atoms in the imidazole ring to give either a neutral or cationic side chain. If cationic, it could make a strong ion-pairing interaction with the phosphate group of LPA, and if neutral, it would donate a hydrogen bond. To assess whether the histidine is protonated on both imidazole nitrogen atoms, we replaced the histidine with glutamine, which can only hydrogen bond but not ion-pair with LPA. The H4.64Q mutant had no impact on the LPA-induced receptor activation, consistent with the hypothesis that the histidine residue is neutral in charge and serves as a hydrogen bond donor to the LPA phosphate (Fig. 2C). Lys-5.37 was chosen as a control residue, and its replacement with alanine had no impact on receptor activation.

LPA$_5$ Model Refinement—Site-directed mutagenesis results revealed some inconsistencies between the experimental impact of the mutations and the predicted electrostatic interactions with the mutated residues in the initial LPA$_5$ model. The discordance between the model and the experimental data occurred in the relative distances between the three arginine residues and the phosphate group. AGP 18:1, as the most potent LPA$_5$ ligand, was selected to guide model refinements. The model was refined by rotating the side chains of Arg-2.60 and Arg-7.32 inward toward the phosphate headgroup of the ligand AGP 18:1 to improve ligand-receptor electrostatic interactions as suggested by the experimental impact of mutations at these sites. The modified receptor model was geometry-optimized and further refined by extending the helical segments of TM6 and TM7 toward the extracellular space by replacing the structure of residues Leu-6.60 to Val-6.66 and Arg-7.30 to Met-7.36, respectively, with ideal helical segments. These modifications gave distances from the phosphate group of LPA 18:1 to Arg-2.60, Arg-6.62, Arg-7.32, and His-4.64 of 2.98, 4.62, 3.20, and 3.03 Å, respectively (Table 2). After refinement, the model
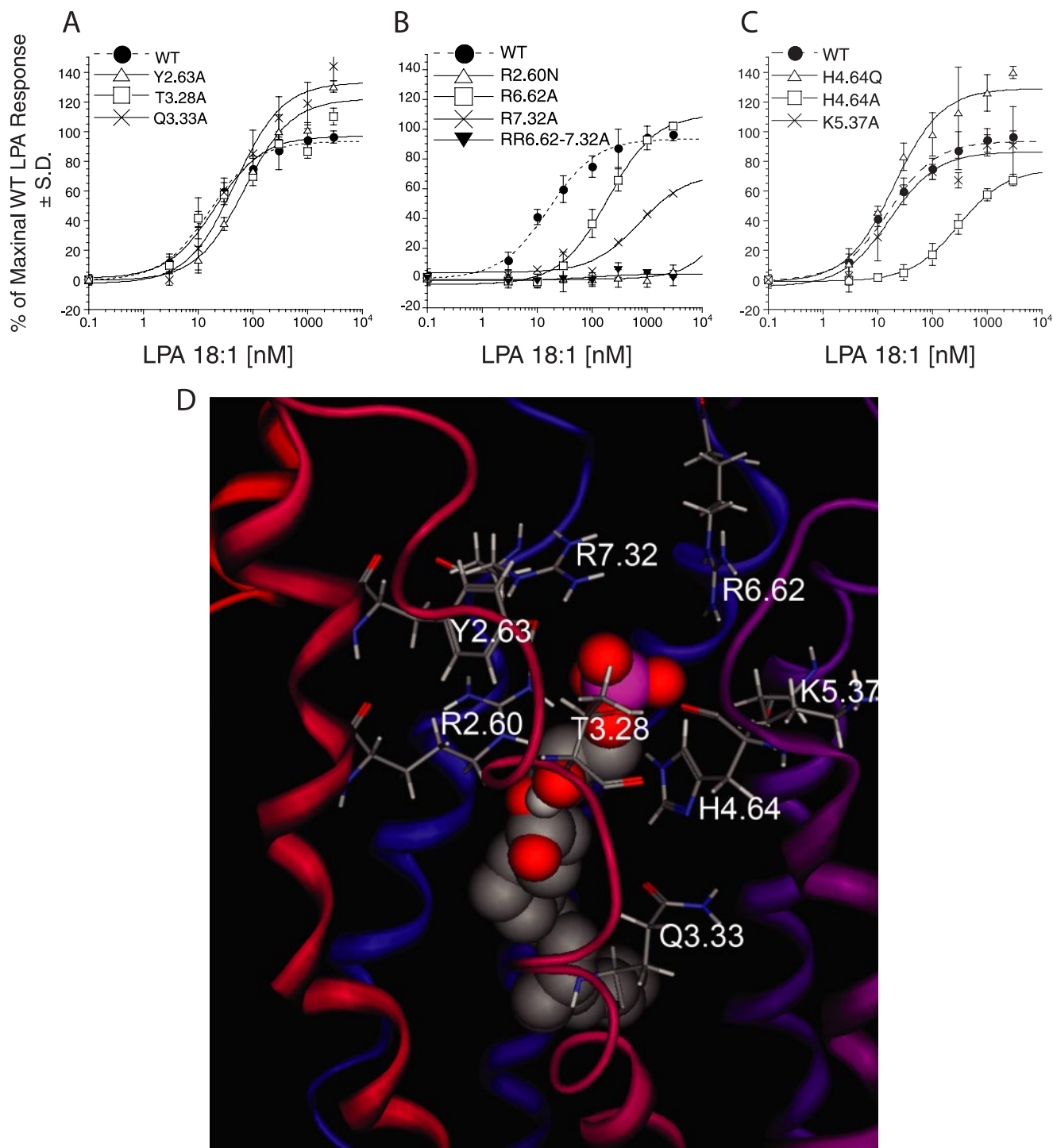
FIGURE 2. **LPA-induced receptor activation of LPA₅ and its mutants and a model of the LPA 18:1 complex with LPA₅.** *A–C,* normalized calcium transients elicited by increasing concentration of LPA 18:1 in RH7777 cells transiently expressing LPA₅ and its mutants. 100% represents the maximal response to LPA 18:1 at LPA₅ WT. Samples were run in triplicate, and the mean ± S.D. was plotted. *D,* close-up view of the phosphate headgroup interactions with LPA₅ residues.

was consistent with the experimental LPA-induced activation of all mutants.

Ligand-induced Activation of LPA₅ Revealed by cAMP Elevation—Activation of LPA₅ increases intracellular cAMP levels (17, 18). Therefore, to confirm the impact of these mutations on ligand recognition, we assessed receptor function using the CRE-luciferase reporter gene assay (Fig. 3). The R2.60N and R6.62A/R7.32A mutations abolished the increase

in luciferase activity by 10 μM LPA; however, they had no impact on the activation of luciferase activity stimulated by 50 μM forskolin. The alanine mutation at Arg-7.32 showed significantly decreased response to 10 μM LPA ($p < 0.05$). For the other mutants the luciferase activity stimulated by 10 μM LPA as well as by 50 μM forskolin was similar to WT. These results were consistent with the refined model and the findings with ligand-induced Ca^{2+} mobilization.

SAR Analysis—We next tested various LPA analogs (Fig. 4) on LPA$_5$ using Ca^{2+} mobilization for a read-out, which provides a sensitive assay with a better dynamic range than the CRE-reporter gene assay. First, we compared the effect of acyl chain length and the degree of unsaturation on ligand properties for seven 1-acyl-LPA analogs. All the analogs tested except for LPA 18:0 and 20:0 showed comparable EC$_{50}$ with LPA 18:1 (Fig. 5*A*). LPA 18:0 and 20:0 showed higher EC$_{50}$ compared with LPA 18:1 (LPA 18:0, EC$_{50}$ = 67.4 ± 4.6; LPA 20:0, EC$_{50}$ > 450; and LPA 18:1, EC$_{50}$ = 11.2 ± 2.1 nM). The overlay of computationally docked phosphate headgroups of these LPA species is shown in Fig. 5*B*, and the modeled interaction distances are shown in Table 2. The distances indicate that each LPA species showed excellent interactions with Arg-2.60 and His-4.64 (distances consistently less than 3 and 3.5 Å, respectively); interactions were weaker with Arg-6.62 and intermediate inter-

TABLE 2
Modeled interaction distances (Å) between select LPA5 residues and ligands

	Arg-2.60	Arg-7.32	Arg-6.62	His-4.64
LPA 18:1	2.98	3.20	4.62	3.03
LPA 18:2	2.93	5.77	6.28	2.82
LPA 18:3	2.75	5.58	6.89	3.16
LPA 20:4	2.83	5.45	6.73	3.04
LPA 16:0	2.94	4.70	5.81	3.13
LPA 18:0	2.66	5.64	6.66	2.93
LPA 20:0	2.50	7.26	9.24	3.43
LPA 18:1	2.98	3.20	4.62	3.03
AGP 18:1	2.84	5.09	5.46	3.04
AGP 16:0	2.95	5.62	6.97	2.86
AGP 18:0	2.68	6.65	7.08	2.75
LPA 18:1	2.98	3.20	4.62	3.03
CPA 18:1	2.82	6.11	7.15	3.24
CPA 16:0	2.89	2.83	5.50	4.87
LPA 18:1	2.98	3.20	4.62	3.03
2CCPA 16:1	3.69	3.95	3.97	6.58
3CCPA 16:1	2.65	2.92	4.42	4.54
LPA 18:1	2.98	3.20	4.62	3.03
2CCPA 18:1	3.28	4.04	4.35	5.12
3CCPA 18:1	3.73	6.61	8.97	3.18
LPA 18:1	2.98	3.20	4.62	3.03
FMP	2.99	3.90	5.60	2.97
FPP	2.80	2.81	4.93	2.73
NAG	3.17	5.77	6.99	3.23

actions with Arg-7.32. These observations are consistent with the experimental observation that these LPA species are agonists. The least potent member of the series, LPA 20:0, showed a difference in the position of the phosphate compared with more potent analogs. The phosphate group of LPA 20:0 was offset, and the distances from several cationic residues, notably Arg-7.32 and Arg-6.62, were greater than to other LPA species, indicating a weaker interaction with the receptor. This poor ionic interaction could be the reason for the poor activation of the receptor.

Next we examined the ligand properties of AGP analogs. AGP 18:1 was ~5-fold more potent than LPA 18:1 (EC$_{50}$ = 2.1 ± 0.9 and 15.1 ± 5.4 nM, respectively), whereas AGP 18:0 was ~4-fold less potent (EC$_{50}$ = 61.9 ± 19.2 nM). The phosphate headgroups of docked individual AGP species have been overlaid (Fig. 6*B*), and the modeled interaction distances are shown in Table 2. As for the LPA species, the measured distances are consistent with the observation that both AGP species activated the receptor. The distances also reflect the poorer potency of AGP 18:0, with significantly longer distances to Arg-7.32 and Arg-6.62 compared with the other AGP species. The greater potency of AGP 18:1 relative to LPA 18:1 is reflected in the models in a more subtle fashion. In particular, the carbonyl group of LPA 18:1 is located in a hydrophobic pocket formed by Phe-3.32 and Met-3.36. Placement of a polar moiety in a nonpolar pocket is entropically unfavorable. Hence, the lack of the carbonyl group in AGP 18:1 is therefore preferred by LPA$_5$.

CPA has been shown to evoke partial cross-desensitization with LPA and to activate LPA$_{1-4}$ receptors (21, 41). For this reason, we also tested the ligand properties of CPA species at LPA$_5$. Although both CPA analogs activated LPA$_5$, CPA 16:0 was a weak agonist (EC$_{50}$ ≥624 nM; E_{max} = 65%) and CPA 18:1 showed ~4-fold higher EC$_{50}$ compared with LPA 18:1 (81.5 ± 22 and 23 ± 6.0 nM, respectively; Fig. 7*A*). We also tested ligand properties of CCPA analogs at LPA$_5$ because CCPAs do not activate LPA$_{1-4}$ (35). All the CCPA analogs tested showed reduced potency compared with LPA 18:1 (Fig. 8*A*). Comparison of the phosphate headgroup positions for LPA 18:1 and CPA species are shown in Fig. 7*B*, and LPA and CCPA species are shown in Fig. 8, *C* and *D*, and distances between the select residues of LPA$_5$ and the ligands are shown in Table 2. The observed close interactions with Arg-2.60 and at least one other residue are consistent with the experimentally observed agonism by CPA and CCPA species. Although distances to the cationic residues are comparable for LPA 18:1 and CPA species, weaker electrostatic interactions would occur for CPA species because of their reduced charge, −1 relative to −2 for LPA 18:1. The poorer potency of CPA 16:0 relative to CPA 18:1, however, is not reflected in the observed distances.
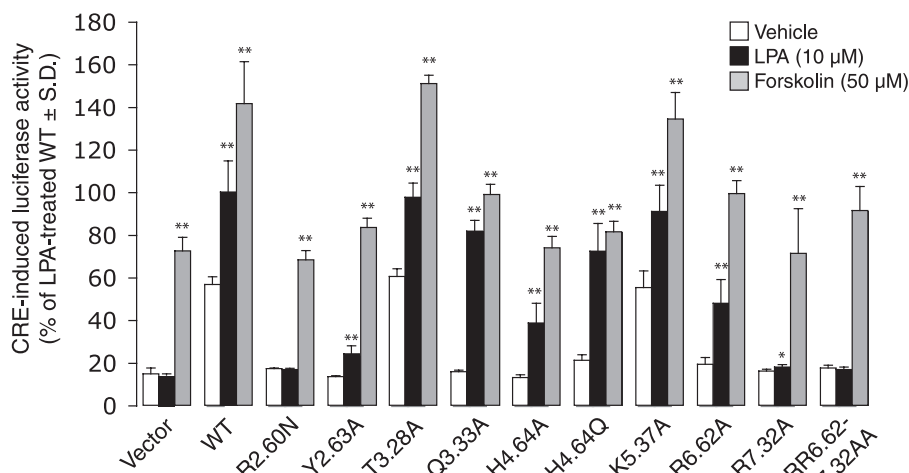

FIGURE 3. **Effect of select mutations on ligand-induced CRE-luciferase activity.** Light units are given as a percentage of the LPA 18:1-treated response in WT LPA$_5$-transfected cells. Samples were run at least in triplicate, and the mean ± S.D. was plotted. *Asterisks* indicate significant differences from the vehicle control in each mutant (*, $p < 0.05$ and **, $p < 0.01$).
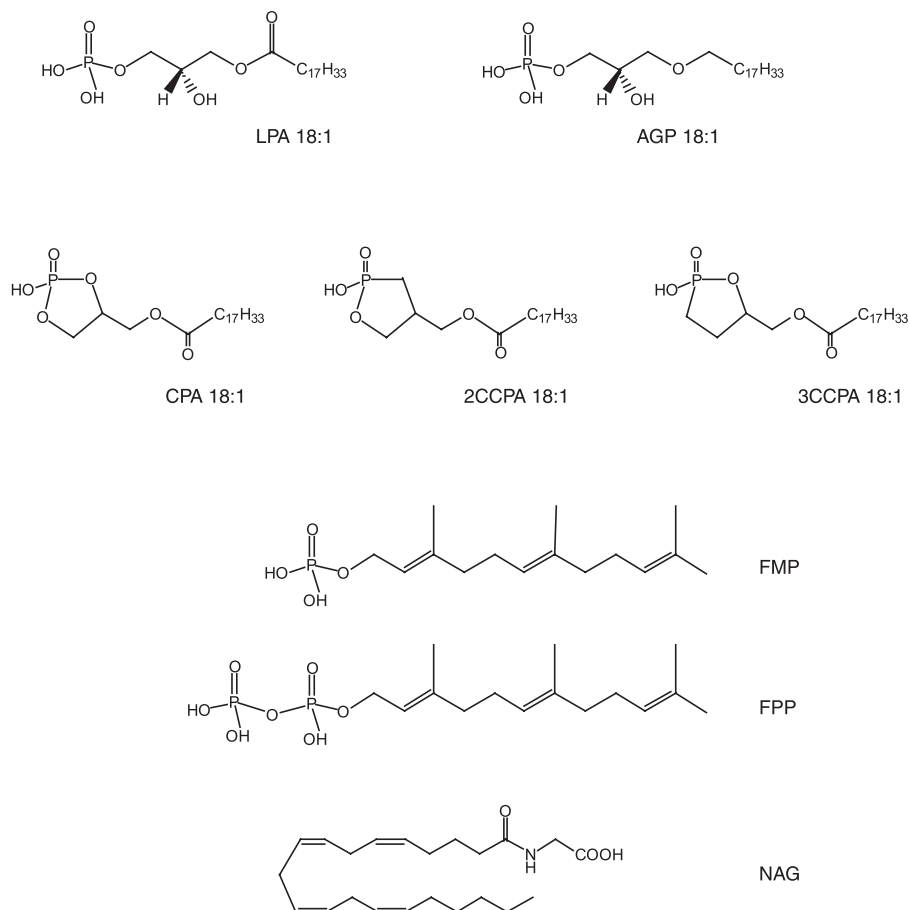
FIGURE 4. **Structures of ligands used in this study.**

our model (Table 2). Based on these predictions, we examined the activation of LPA$_5$ by NAG, FPP, and FMP, which we had earlier identified as endogenous antagonists of EDG LPA receptors (42). Among this subset of ligands, LPA 18:1 was the most potent in mobilizing Ca^{2+} in RH7777 cells transiently transfected with LPA$_5$ (Fig. 9*A* and Table 3). Activation by NAG did not saturate at the highest concentration we tested, 10 μM. FMP showed partial agonist activity with E_{max} of 60% that of LPA 18:1. FPP was a full agonist; however, its EC$_{50}$ was ~5-fold higher than that for LPA 18:1 (40 $\pm$ 15 *versus* 8.9 $\pm$ 0.7 nM, respectively). To confirm this result, we examined the effects of these ligands on the CRE-directed luciferase activity in RH7777 cells transiently expressing LPA$_5$ (Table 4). LPA18:1 was the most potent activator of CRE-luciferase; FPP and FMP both showed reduced potency. In contrast, NAG failed to increase significantly luciferase activity compared with vehicle. These results were consistent with the predictions of our refined model and also with the results obtained with ligand-induced Ca^{2+} mobilization.

To expand the SAR of LPA$_5$, we applied a set of previously identified agonists and antagonists of the EDG family LPA receptors to re-evaluate their pharmacological properties. Table 5 shows the list of compounds that activate LPA$_5$. In this list of 12 compounds, FMP and FPP stand out as selective agonists of LPA$_5$ with EC$_{50}$ values in the nanomolar range. Although we found several other agonists that activated LPA$_5$, these were not full agonists when tested up to 3 μM. As the farnesyl phosphates and NAG had not previously been computationally examined at LPA$_{1-3}$, these compounds were docked into both active and inactive models of each receptor as done previously to investigate stereochemical effects on pharmacological profiles (43). The computational results indicated that antagonism is observed for receptor:ligand pairs when either the ligand shows an energetic preference for the inactive receptor model coupled with strong electrostatic interactions with critical ion-pairing residues and good van der Waals contact with hydrophobic residues or an energetic preference for the active receptor model without completely filling the putative hydrophobic binding pocket. Partial agonism was observed only for NAG at the LPA$_2$ receptor and was reflected in an energetic preference for the active receptor model, and weak contacts with all critical charged residues, as well as the potential to extend deeper into the hydrophobic pocket than either FMP or FPP. The computational results were also consistent with the receptor:ligand combinations showing no effect, with

During the preparation of this manuscript, Oh da *et al.* (22) reported that FPP and NAG were endogenous ligands for LPA$_5$. Moreover, in their system, FPP was more potent than LPA, whereas NAG was as potent as LPA in activating LPA$_5$. Their computational modeling combined with site-directed mutagenesis of LPA$_5$ indicated that four residues, Thr-97 (Thr-3.28), Gly-98 (Gly-3.29), Phe-101 (Phe-3.32), and Arg-276 (Arg-7.32), were responsible for the interaction of LPA$_5$ with these ligands. Therefore, we examined the ligand-receptor interactions of these residues within our model. The docked complexes of FMP, FPP, and NAG all showed weak interactions with Gly-3.29 within 7.34, 8.98, and 6.02 Å. Mutation of glycine may have had structural consequences that were not considered in the previous study. The model did not predict hydrogen bonding of the hydroxyl group of Thr-3.28 with FMP, FPP, or NAG as the interaction distances were 3.42, 5.43, and 4.66 Å, respectively. Our computational model predicted FPP to be a more potent ligand than FMP based on closer interaction distances (Table 2). Oh da *et al.* (22) reported the F3.32W mutant reduced sensitivity to FPP to a level 10-fold lower than WT, whereas F3.32A mutant did not change sensitivity to FPP. FPP interaction with Phe-3.32 in our model suggests that F3.32W would block the binding pocket, whereas F3.32A would keep the pocket open for ligand binding. The docking simulations also predicted NAG to be a weak activator of the LPA$_5$ based on weak interactions with the mutated residues Arg-2.60, Arg-6.62, Arg-7.32, and His-4.64 within the binding pocket of

A

B

FIGURE 5. **SAR for 1-acyl-LPA analogs at LPA$_5$ and model of the receptor-ligand complexes.** *A,* intracellular Ca^{2+} transients were measured in response to different 1-acyl-LPA species in RH7777 cells transiently expressing LPA$_5$. 100% represents the maximal response to LPA 18:1. Samples were run in triplicate, and the mean ± S.D. was plotted. *B,* comparison of docked phosphate headgroups for LPA18:1 (*light green*), 18:2 (*dark green*), 18:3 (*light yellow*), 20:4 (*dark yellow*), 16:0 (*orange*), 18:0 (*red*), and 20:0 (*purple*).
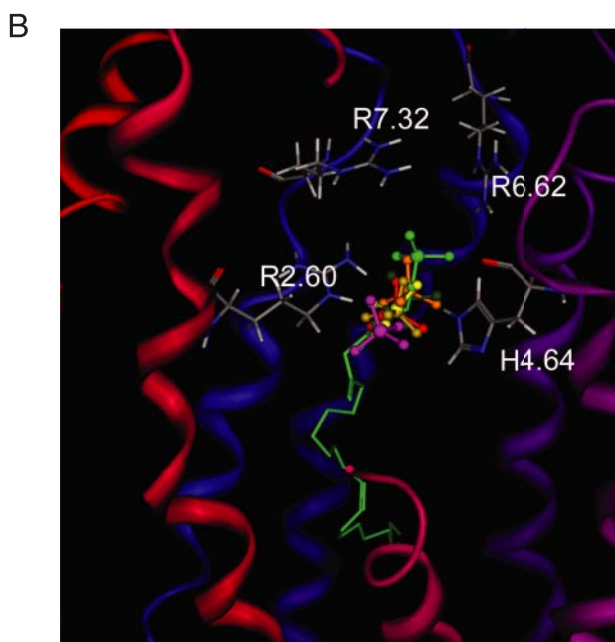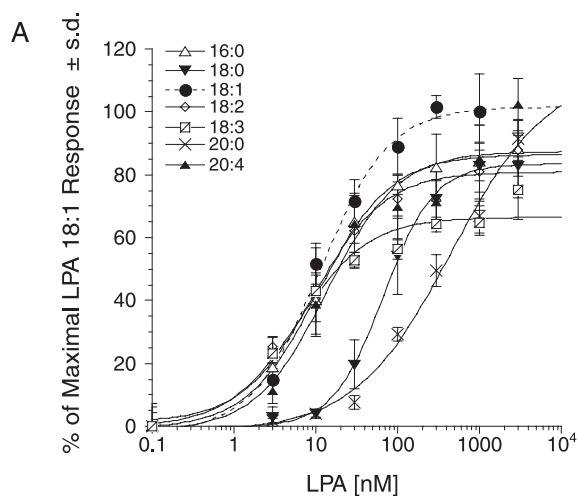

A

B

FIGURE 6. **SAR for 1-alkyl-LPA analogs at LPA$_5$ and model of the receptor-ligand complexes.** *A,* intracellular Ca^{2+} transients were measured in response to different 1-alkyl-LPA species in RH7777 cells transiently expressing LPA$_5$. 100% represents the maximal response to LPA 18:1. Samples were run in triplicate, and the mean ± S.D. was plotted. *B,* comparison of docked phosphate headgroups for LPA 18:1 (*green*) and AGP species (*yellow,* 18:1; *orange,* 16:0; *red,* 18:0).

distances to critically important residues in the preferred receptor model over 10 Å (data not shown).

Agreement of the Predictions Based on the Mutant Protein Modeling and Experimental Properties of Additional Mutants—Models of LPA$_5$ mutants were generated to validate the refined model. The docked complexes with the lowest binding energies are shown in Fig. 10, *A–D*. The polar side chains at the mutation sites of L5.41N and L5.45N were in close proximity to the glycerol backbone (3.65 Å) and hydrophobic tail (3.46 Å) of LPA, respectively. We hypothesize that LPA would displace solvating waters from these polar residues during binding, which is an entropically unfavorable process. This modeling result is consistent with the poorer potency of LPA for these two mutants relative to the WT LPA$_5$ (Fig. 10*E*). Although we have previously demon-
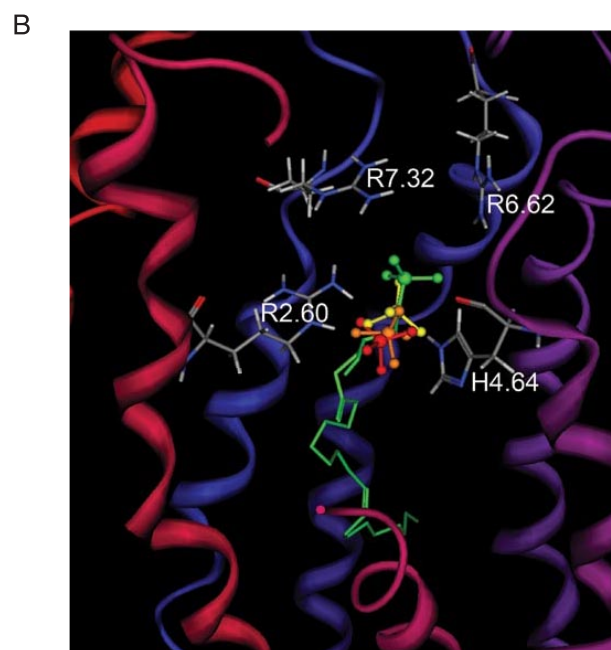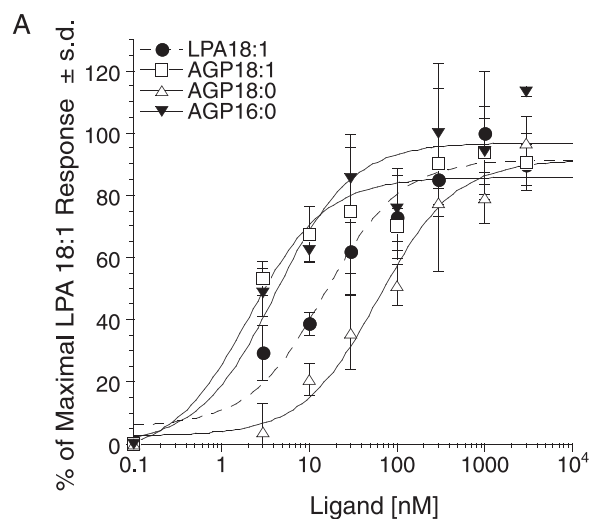
strated that differences in expression levels over a wide range have no effect on ligand potency (14), the unexpectedly low expression of the L5.45N mutant (Table 1) might affect the EC$_{50}$ and/or E$_{max}$ values. The polar side chains at the mutation sites of the L7.35N and V7.39N mutants showed favorable hydrogen bonding interactions with LPA, displaying interatomic distances of 2.79 and 3.08 Å, respectively. However, the added hydrogen bond in each of these mutants failed to compensate for the decreased strength of interactions between the phosphate group and the surrounding amino acid residues. In the case of L7.35N, a decreased ion-pairing interaction with Arg-7.32 (5.63 Å *versus* 3.20 Å in the WT complex) occurs as a consequence of the mutation. Ion-pairing interactions in proteins are of greater magnitude
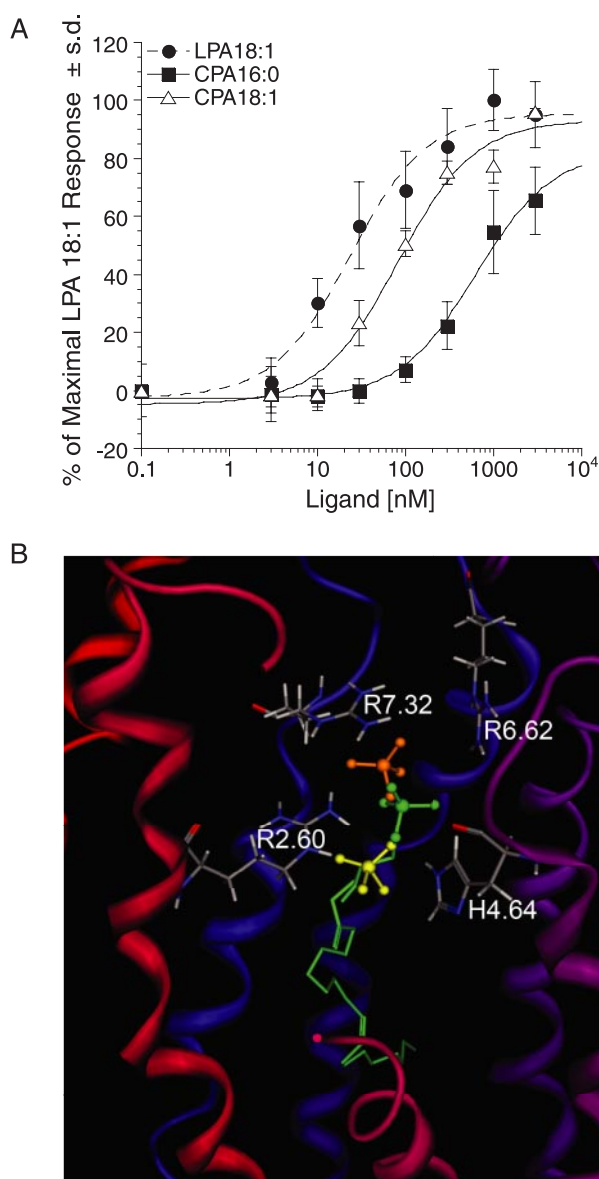
A

B

FIGURE 7. **SAR for CPA analogs at LPA$_5$ and model of the receptor-ligand complexes.** *A,* intracellular Ca^{2+} transients were measured in response to CPA analogs in RH7777 cells transiently expressing LPA$_5$. 100% represents the maximal response to LPA 18:1. Samples were run in triplicate, and the mean ± S.D. was plotted. *B,* comparison of docked phosphate headgroups for LPA 18:1 (*green*) and CPA species (*yellow,* 18:1; *orange,* 16:0).

than hydrogen bonds, and thus the overall effect predicted is a decrease in potency. Experimental data of LPA 18:1-induced intracellular Ca^{2+} mobilization showed that L7.35N caused 20-fold increase in EC$_{50}$ (Fig. 10*E*). In the case of V7.39N, an increased distance between His-4.64 and the anionic headgroup (4.85 Å *versus* 3.03 Å in the WT complex) reflects a decrease in hydrogen bonding to the phosphate. A hydrogen bond of similar distance involving the anionic phosphate group is stronger than a hydrogen bond involving an uncharged oxygen atom such as the ester oxygen atom of LPA. This is consistent with the decrease in binding affinity experimentally manifested as a 30-fold shift in EC$_{50}$ (Fig. 10*E*). These results altogether indicate our refined model of LPA$_5$ is reliable and has a predictive power.

Pharmacophore Model Development of LPA$_5$ and Lead Evaluation—Lipids are often poor drug candidates because of poor bioavailability and the poor selectivity that results from their intrinsic flexibility. Therefore, the identification of novel non-lipid compounds is needed. For this reason, we developed a pharmacophore model of LPA$_5$ for *in silico* screening (Fig. 11). The detailed method of developing the pharmacophore model is described under "Experimental Procedures." Fourteen pharmacophore hits (supplemental Fig. 2) were tested in the Ca^{2+} mobilization assay. Compound H2L 5987411 was identified as a partial antagonist of LPA$_5$ with an IC$_{50}$ of 3.5 μM and 42% maximal inhibition at 30 μM (Table 6). This compound was also an antagonist of LPA$_4$ with an IC$_{50}$ of 1.4 μM and 46% maximal inhibition, although it did not have effect on LPA$_1$, LPA$_2$, or LPA$_3$. We also identified H2L 5765834 as an LPA$_5$ antagonist. This compound was originally identified based on its similarity to an LPA$_3$ receptor antagonist[3] and emerged as an LPA$_{1,3,5}$ antagonist during selectivity screening (Table 6). H2L 5765834 did not match the automated conformational search of the pharmacophore, but it matched the pharmacophore using a relaxed chemical feature definition in which the centroid of the aromatic ring was equated to a hydrogen bond acceptor site.

Effect of LPA$_5$ Agonists and Antagonists on Platelet Activation—LPA$_5$ represents the most abundant LPA receptor mRNA transcript in human platelets (28). Therefore, we examined the effects of the LPA$_5$ agonists (Table 5) and antagonists (Table 6) that we identified in this study on LPA-induced platelet shape change (Table 7). Octadecenyl phosphate, which activates LPA$_5$ and partially also LPA$_4$ at micromolar concentrations (Table 5), was almost as potent as the physiological agonist AGP 18:1, and it induced platelet shape change with an EC$_{50}$ value of 2 nM. FPP and FMP activated platelets with 100 times higher concentrations (EC$_{50}$ values of 0.29 and 0.21 μM, respectively) than AGP 18:1. 2CCPA 16:1 and 3CCPA 16:1, which partially activated LPA$_5$ at micromolar concentrations, were weak partial agonists for platelets. Octyl thiophosphatidic acid, which selectively activated LPA$_5$, induced platelet shape change with an EC$_{50}$ of 2.1 μM. NAG lacked agonistic and antagonistic activity. The compounds that induced platelet activation also inhibited shape change to subsequent application of 20 nM LPA after a preincubation for 30 min. Because platelet LPA receptors show a homologous desensitization 5 min after activation (24), it is likely that the LPA$_5$ activating compounds might have achieved their inhibition through desensitizing LPA receptors rather than through receptor antagonism. In support of this hypothesis, the true antagonists, H2L 5987411 and H2L 5765834, did not elicit shape change when applied alone, but they inhibited LPA-induced platelet shape change. All compounds had no effect on ADP-elicited platelet activation.

DISCUSSION

The recent expansion of the LPA receptor family with members of the purinergic cluster presented the opportunity to examine the principles of LPA recognition by eight different
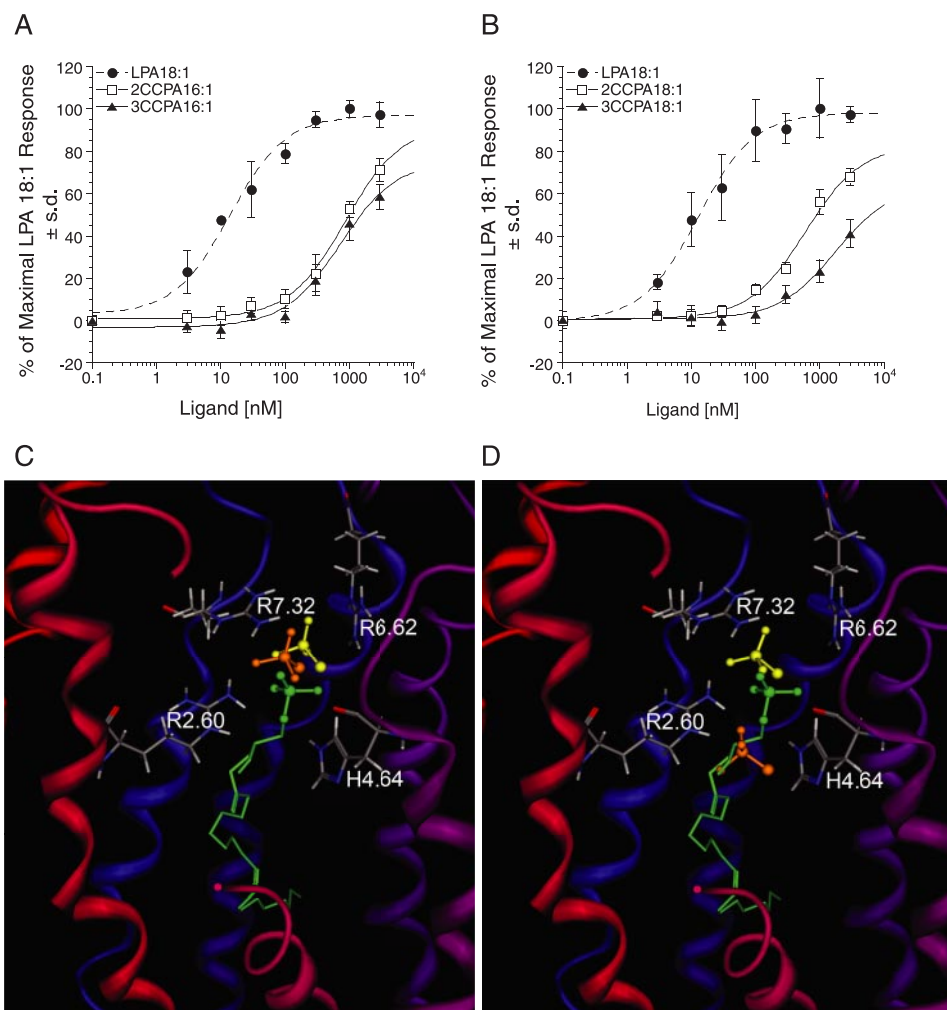
FIGURE 8. **SAR for CCPA analogs at LPA$_5$ and model of the receptor-ligand complexes.** *A* and *B,* intracellular Ca^{2+} transients were measured in response to CCPA 16:1 analogs (*A*) and CCPA 18:1 analogs (*B*) in RH7777 cells transiently expressing LPA$_5$. 100% represents the maximal response to LPA 18:1. Samples were run in triplicate, and the mean ± S.D. was plotted. *C,* comparison of docked phosphate headgroups for LPA 18:1 (*green*) and CCPA 16:1 species (*yellow,* 2-carba; *orange,* 3-carba). *D,* phosphate headgroup comparison of docked LPA 18:1 (*green*) and CCPA 18:1 species (*yellow,* 2-carba; *orange,* 3-carba).

dantly support that LPA is the preferred agonist of GPR92 over FMP, FDP, and NAG justifying the proposed terminology of LPA$_5$ for this GPCR.

Our previous studies on ligand-receptor interactions in the LPA$_{1-3}$ EDG family LPA receptors showed that Arg-3.28 ion-pairs with the phosphate of LPA, and mutation to alanine abolishes the ionic interaction and LPA-induced receptor activation in all three EDG family LPA receptors (14, 16, 21). This residue is also conserved in the S1P-EDG receptors and has been found to abolish ligand activation when mutated to alanine in S1P$_1$ and S1P$_4$ (16, 39, 40). Thus, Arg-3.28 is a critical residue for ligand recognition of both LPA and S1P EDG family receptors. The residue in the corresponding position is neither cationic nor involved in LPA recognition in the LPA$_5$ receptor as demonstrated by the WT activity of the T3.28A mutant in this study (Fig. 1 and Fig. 2*A*).

Lys-5.38 is conserved in the EDG family S1P receptors and has been shown to ion-pair with the phosphate of S1P in S1P$_1$ and S1P$_4$, although it is essential for S1P recognition only in S1P$_4$ (36, 40). In EDG family LPA receptors, 5.38 is an arginine in both LPA$_2$ and LPA$_3$, and the residue ion-pairs with the phosphate of LPA, whereas an aspartate at this position in LPA$_1$ does not contribute to ligand activation (14, 21). However, the D5.38R mutant in LPA$_1$ increased receptor activation suggesting the importance of this polar interaction in LPA-EDG receptors. In LPA$_5$, a positively charged lysine occurs at 5.37 instead of 5.38, and this residue is not critical for receptor activation (Fig. 2*C*).

Another positively charged lysine residue in TM7 in S1P$_1$ (Arg-7.34) has been demonstrated to form a critical interaction with the phosphate of S1P (39). In LPA$_{1-3}$, position 7.36 is occupied by a positively charged lysine in LPA$_1$ and LPA$_2$ and an arginine in LPA$_3$. The K7.36A mutant diminished the activation of LPA$_2$ but enhanced the activation of LPA$_1$. R7.36A mutant had no effect on receptor activation of LPA$_3$; however, alanine mutation of the adjacent residue in LPA$_3$, Lys-7.35, significantly diminished activation, suggesting that Lys-7.35 but not Arg-7.36 in LPA$_3$ forms cationic interactions with the LPA phosphate group (14, 21). The arginine residue in TM7 of LPA$_5$, Arg-7.32, now defines a fourth TM7 location where an inward-facing cationic residue can be placed for favorable interactions with the phosphate group of phospholipid ligands.

seven transmembrane receptors. Here we sought to determine whether GPR92/LPA$_5$ specifically and preferentially recognizes LPA among a host of naturally occurring agonists and to understand the structural foundation of its ligand recognition and SAR. We applied a previously successful approach utilizing an iterative process of model building, experimental validation, and model refinement, and we arrived at a model that shows consistency with all the experimental SAR and site-directed mutagenesis data. We began by focusing on amino acid residues that interact with the polar headgroup of LPA. This strategy is based on the expectation that mutations impacting the strongest intermolecular interactions will result in robust alteration in ligand activation and unambiguously aid model refinement. Successive mutagenesis examined weaker interactions selected based on a refined model and showed that this model exhibits qualitative accuracy in predicting the impact of mutations. LPA$_5$ shares less than 20% of amino acids with LPA$_{1-3}$ EDG family LPA receptors. Phylogenetic analysis indicated that LPA$_5$ is more closely related to the LPA$_4$ receptor (17, 18). The predictions of the model and the experimental findings concor-

The present study on a non-EDG family LPA receptor, LPA$_5$, identified three positively charged residues in TM2, -6 and -7, as well as a hydrogen bond donating residue in TM4, involved in ligand recognition. Asparagine mutation at Arg-2.60 abol-
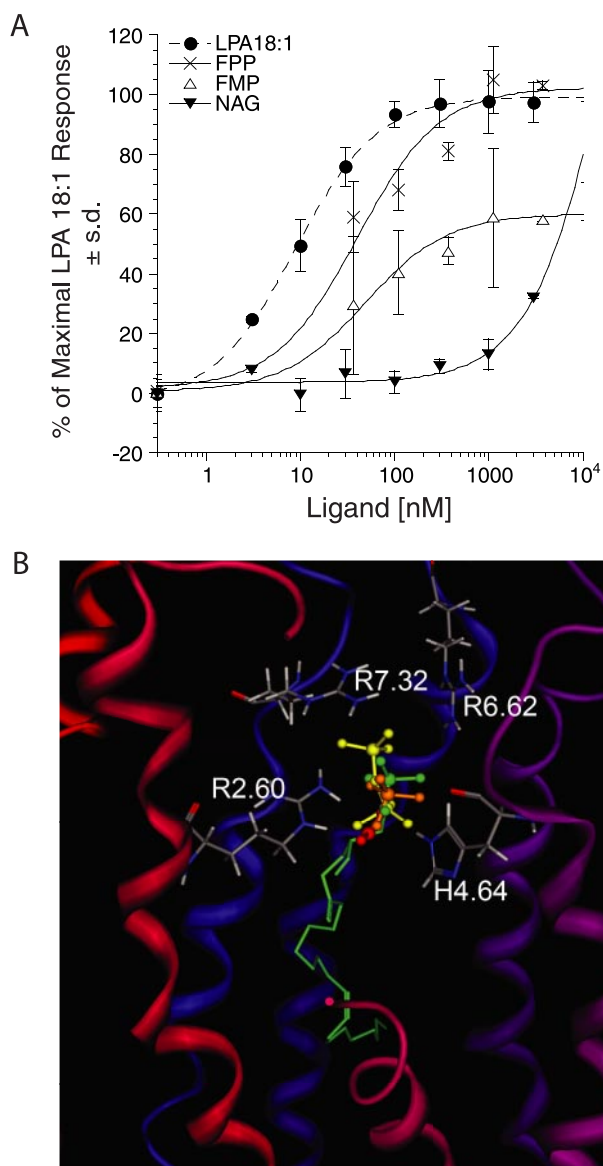

FIGURE 9. **Ligand-induced receptor activation of LPA$_5$ and its mutants.** *A,* normalized calcium transients elicited by increasing concentration of LPA 18:1, FPP, FMP, and NAG in RH7777 cells transiently expressing LPA$_5$ and its mutants. 100% represents the maximal response to LPA 18:1 at LPA$_5$ WT. Samples were run in triplicate, and the mean ± S.D. was plotted. *B,* comparison of docked phosphate headgroups for LPA 18:1 (*green*), FMP (*orange*), FPP (*yellow*), and NAG (*red*).

ished LPA-induced receptor activation, indicating that this arginine is critical for ligand recognition in LPA$_5$. The R7.32A mutant also greatly diminished but did not abolish the activation of the receptor, whereas R6.62A had less impact compared with R7.32A on receptor activation. These results suggest that two arginines at TM6 and -7 are involved in ligand recognition but are not individually essential. However, the double mutation at 6.62 and 7.32 abolished receptor activation demonstrating that the phosphate headgroup interaction with arginine 2.60 is not sufficient for ligand-induced activation. Interestingly, only position 2.60 is occupied by a cationic residue in all members of the LPA$_{4-8}$ receptor cluster, consistent with its more critical role relative to the arginine residues at positions 6.62 and 7.32, which are found in only three receptors of this cluster.

SAR of various LPA species and AGP analogs revealed that the different ligand-receptor interaction distances are consistent with the receptor activation potency of the ligands (Figs. 5 and 6 and Table 2); however, to thoroughly understand the ligand recognition of the receptor, validation and refinement of the hydrophobic interactions are necessary in future experiments. Kotarsky *et al.* (17) reported potency and efficacy of some phospholipids on LPA$_5$. Surprisingly, the order of potencies for LPA analogs with different chain length showed that LPA 14:0 or LPA 16:0 had higher potency than LPA 18:0 or LPA 18:1. However, the results obtained from ligand binding assay showed that LPA 18:1 was the most potent among the LPA species they tested. CCPA is a metabolically stabilized derivative of CPA with a methylene group at either the *sn*-2 or *sn*-3 position replacing a phosphate oxygen (Fig. 4). Previously, we identified CCPA analogs as novel inhibitors of metastatic cancer that inhibit LPA production by the enzyme autotaxin, a tumor cell autocrine motility factor (35). We have also reported that CCPA analogs neither significantly activate nor inhibit the LPA$_{1-4}$ receptors. The present results necessitate the revision of this concept and also raise the possibility that the profound *in vivo* anti-metastatic activity of CCPA is not only because of the inhibition of lysophospholipase D/autotaxin but also to activation of LPA$_5$.

The reduced potency of CPA analogs compared with LPA 18:1 can be attributed to the inability of the disubstituted phosphate to adopt a −2 charge, thus reducing its electrostatic interaction with the surrounding cationic residues from TM2, -6, and -7 (Fig. 7). However, CPA 18:1 activates LPA$_5$ relatively strongly compared with the EDG LPA receptors (21, 35). We found a major difference between LPA$_{1-4}$ and LPA$_5$ in that all CCPA analogs activated LPA$_5$, albeit with lower potency com-

TABLE 3

EC$_{50}$ and E_{max} values of LPA 18:1, FPP, FMP, and NAG for WT and mutants

NS indicates that the response did not saturate at the highest concentration tested (3 μM for WT and 10 μM for FPP, FMP, and NAG). NA indicates that the receptor activation was not detected up the highest concentration tested (3 μM for WT and 10 μM for FPP, FMP, and NAG).

Receptor	EC$_{50}$ (nM)				E_{max} (%)			
	LPA 18:1	FPP	FMP	NAG	LPA 18:1	FPP	FMP	NAG
Wild type	8.9 ± 0.7	40 ± 15	49 ± 13	NS	100	102 ± 5.2	60 ± 2.3	32 ± 0.57
R2.60N	NA	NA	NA	NA				
H4.64A	NS	210 ± 78	174 ± 71	NA	67 ± 3.8	95 ± 4.9	77 ± 4.6	
R6.62A	191 ± 25	NS	NA	NA	110 ± 3.4	13 ± 10		
R7.32A	NS	NA	NA	NA	57 ± 4.2			

TABLE 4

Effect of LPA 18:1, FPP, FMP, and NAG (10 μM, respectively) on CRE-mediated luciferase activity in RH7777 cells transiently expressing the WT and mutants

Receptor	CRE-induced luciferase activity (% of LPA 18:1 in WT)				
	Vehicle	LPA 18:1	FPP	FMP	NAG
Vector	26 ± 1.9	26 ± 2.9	27 ± 3.1	28 ± 1.2	26 ± 1.9
Wild type	68 ± 6.0	100 ± 17	91 ± 5.1	88 ± 5.8	67 ± 9.7
R2.60N	22 ± 0.5	22 ± 0.6	21 ± 0.6	22 ± 0.3	21 ± 0.2
H4.64A	25 ± 0.7	53 ± 6.9	93 ± 6.6	38 ± 3.2	25 ± 1.4
R6.62A	25 ± 1.4	47 ± 5.2	25 ± 1.6	24 ± 1.4	25 ± 0.3
R7.32A	23 ± 1.3	25 ± 1.3	22 ± 0.9	23 ± 0.4	22 ± 0.9

pared with LPA 18:1. The reduced potency of CCPA analogs can be attributed to the replacement of one of the oxygens with carbon reducing its electrostatic interaction with the surrounding cationic residues near the phosphate headgroup.

During the course of this study, Oh da *et al.* (22) reported that they found FPP and NAG activate LPA$_5$. The activity of FPP and FMP was not surprising as farnesyl phosphates had previously been identified as ligands of LPA targets, including LPA$_2$, LPA$_3$, and peroxisome proliferator-activated receptor-γ (42). The FPP, FMP, and NAG are naturally occurring agents. FPP and FMP are intermediates in the biosynthesis of steroids, carotenoids, the side chain of ubiquinones, and polyisoprenoids, as

TABLE 5

Pharmacological evaluation of the previously identified LPA receptor agonists and antagonists on LPA$_5$ receptor

RH7777 cells stably expressing LPA$_{1-3}$ or transiently expressing LPA$_5$ and CHO cells stably expressing LPA$_4$ were used to measure intracellular Ca^{2+} mobilization. NE indicates no effect up to 30 μM. NS indicates nonsaturated at the highest concentration (3 μM for LPA$_5$ and 10 μM for LPA$_4$). E_{max} indicates % of maximal LPA 18:1 response. PA indicates partial antagonist.

| Name	Structure	LPA$_1$	LPA$_2$	LPA$_3$	LPA$_4$	LPA$_5$
LPA 18:1		EC$_{50}$:130nM E_{max}: 100%	EC$_{50}$:3nM E_{max}: 100%	EC$_{50}$:81nM E_{max}: 100%	EC$_{50}$:245nM E_{max}: 100%	EC$_{50}$:15nM E_{max}: 100%
AGP 18:1		EC$_{50}$:1.5μM E_{max}: 100%	EC$_{50}$:101nM E_{max}: 108%	NS E_{max}: 63%	EC$_{50}$:303nM E_{max}: 98%	EC$_{50}$:2nM E_{max}: 97%
Diacylglycerol pyrophosphate		IC$_{50}$:5.5μM	NE	IC$_{50}$:454nM	NE	NS E_{max}: 39%
Carba-cyclic phosphatidic acid (2CCPA 16:1)		NS E_{max}: 13%	NE	NS E_{max}: 14%	NE	NS E_{max}: 71%
Carba-cyclic phosphatidic acid (3CCPA 16:1)		NE	NE	NE	NE	NS E_{max}: 58%
N-palmitoyl tyrosine phosphoric acid		IC$_{50}$:3.45μM	NE	NE	NE	NS E_{max}: 70%
LPA-methylene phosphonate		PA	IC$_{50}$:1.42μM	PA	EC$_{50}$:5.4μM E_{max}: 29%	NS E_{max}: 59%
LPA-bromomethylene phosphonate		IC$_{50}$:1.62μM	IC$_{50}$:1.42μM	IC$_{50}$:1.16μM	IC$_{50}$:266nM	NS E_{max}: 45%
Octanamido-octylamino-oxopropyl dihydrogen phosphate		NE	NE	IC$_{50}$:935nM	NE	NS E_{max}: 36%
Octyl thio-phosphatidic acid		IC$_{50}$:382nM	NE	IC$_{50}$:184nM	NE	NS E_{max}: 92%
Octadecenyl-phosphate		NE	NE	NE	EC$_{50}$:608nM E_{max}: 57%	NS E_{max}: 86%
Farrnesyl pyrophosphate (FPP)		NE	IC$_{50}$:21μM	IC$_{50}$:46μM	IC$_{50}$:1.98μM	EC$_{50}$:40nM E_{max}: 102%
Farnesyl monophosphate (FMP)		NE	IC$_{50}$:161ñM	IC$_{50}$:517nM	IC$_{50}$:1.45μM	EC$_{50}$:49nM E_{max}: 60%
N-arachidonyl glycine (NAG)		IC$_{50}$:757nM	NS E_{max}: 59%	IC$_{50}$:606nM	IC$_{50}$:598nM	NS E_{max}: 32%
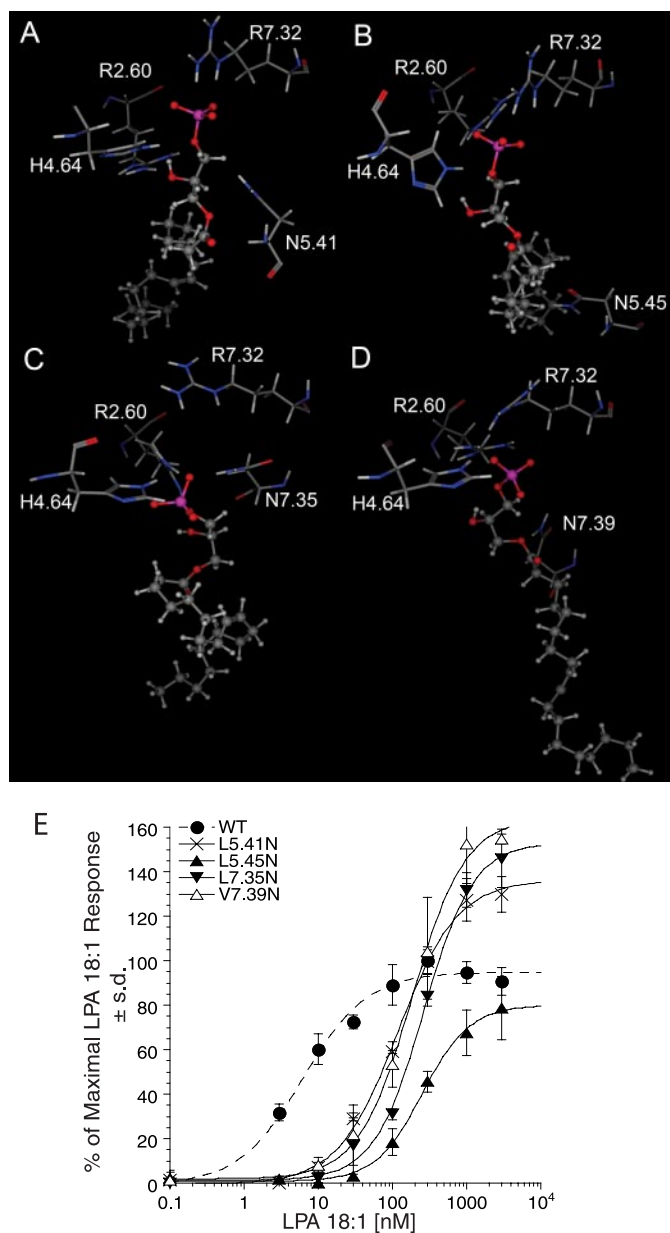
FIGURE 10. **Models of LPA$_5$ mutants and activation by LPA.** LPA 18:1 complexes with LPA$_5$ mutants are shown. LPA 18:1 is shown as a *ball and stick model*; select residues from each LPA$_5$ mutant are shown as *stick models* and labeled. *A,* LPA$_5$ L5.41N mutant. *B,* LPA$_5$ L5.45N mutant. *C,* LPA$_5$ L7.35N mutant. *D,* LPA$_5$ V7.39N mutant. *E,* normalized calcium transients elicited by increasing concentration of LPA 18:1 in RH7777 cells transiently expressing LPA$_5$ and its mutants. 100% represents the maximal response to LPA 18:1 at LPA$_5$ WT. Samples were run in triplicate, and the mean $\pm$ S.D. was plotted.

FIGURE 11. **Pharmacophore model of LPA$_5$.** Overlay of docked LPA$_5$ agonists AGP 18:1 shown in stick with AGP 16:0, LPA 18:1, LPA 18:3, and CPA 18:1 shown in line, used to develop agonist pharmacophore. The anionic, hydrogen bond donor, and hydrophobic regions are colored *purple, pink,* and *blue*. The distances among the three points within the pharmacophore are 3–5 Å from the anionic to hydrogen bond donor region, 8–11 Å from hydrogen bond donor to hydrophobic region, and 12–14 Å from hydrophobic to anionic region.

well as the donor of the farnesyl group for isoprenylation of many proteins (44). NAG is a carboxylic acid analog of the endocannabinoid anandamide, present in the brain as well as in peripheral sites, and shows activity against tonic pain (45). In their assay systems using CV-1 and F11 rat embryonic neuroblastoma $\times$ DRG neuron hybrid cells, FPP was more potent than LPA 18:1, and NAG was as potent as LPA 18:1 in activating LPA$_5$. Our findings using RH7777 cells are not consistent with their data. The receptor activation results obtained from Ca^{2+} mobilization as well as CRE reporter gene assays revealed that acyl and alkyl ether LPA analogs were more potent than FPP,
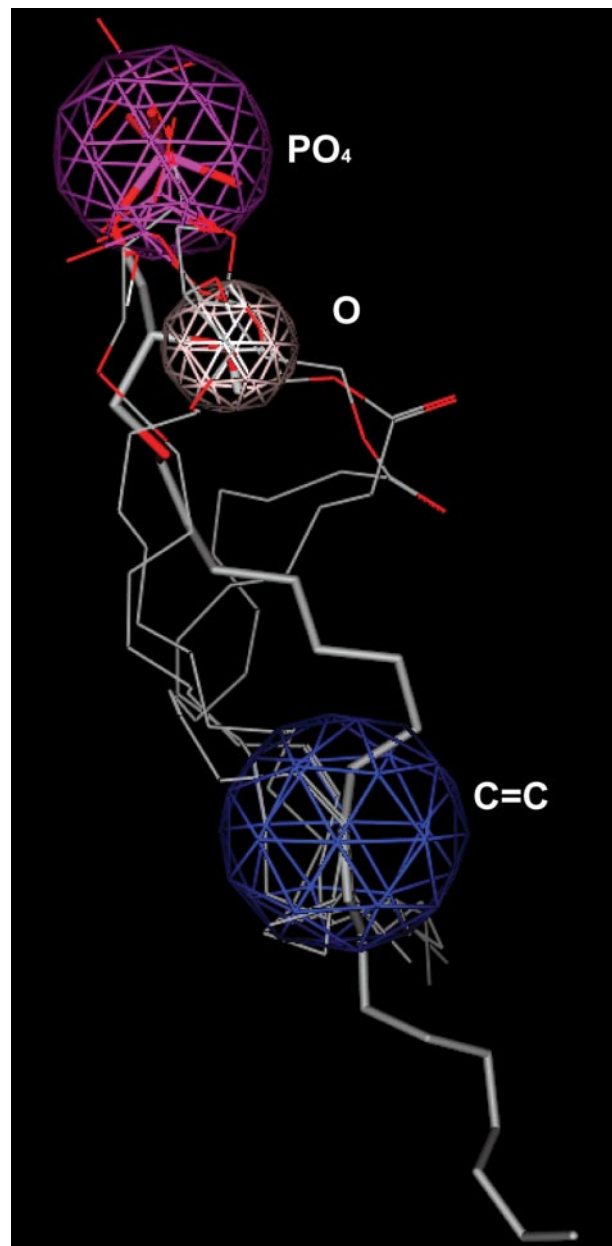
FMP, or NAG with EC$_{50}$ values of 14.8 $\pm$ 3.2 nM for LPA 18:1 (mean values of independent experiments ($n = 6$)), 2.1 $\pm$ 0.9 nM for AGP 18:1, and 4.1 $\pm$ 2.1 nM for AGP 16:0. In contrast, Oh da *et al.* (22), using SRE-luciferase reporter gene assay and inositol trisphosphate production, reported that the EC$_{50}$ values of FPP, the most potent ligand, were 0.26 and 0.38 μM, respectively (22). Thus, agonist-induced intracellular Ca^{2+} mobilization gives superior sensitivity and dynamic range compared with the SRE-luciferase reporter gene assay. Furthermore, the differences between the cell type used for heterologous expression should be carefully considered. The RH7777 cells we used are

TABLE 6

Pharmacological evaluation of the compounds identified by *in silico* screening on LPA receptors
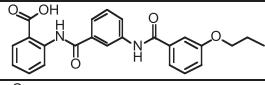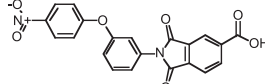
NE indicates no effect.

Compound	Structure	LPA receptor activation Based on Ca assays				
		LPA_1	LPA_2	LPA_3	LPA_4	LPA_5
5987411		NE	NE	NE	$IC_{50}=1.4\mu M$ $Ki=741nM$	$IC_{50}=3.5\mu M$ $Ki=1.3\mu M$
5765834		$IC_{50}=94nM$ $Ki=48nM$	NE	$IC_{50}=752nM$ $Ki=230\ nM$	NE	$IC_{50}=463nM$ $Ki=292nM$

TABLE 7

Effect of LPA_5 agonists and antagonists on platelets

E_{max} indicates maximal shape change induced by drug/shape change induced by 20 nM acyl-LPA 18:1. Shape change induced by 20 nM LPA was 83 ± 15% (mean ± S.D., n = 3) of maximal and set to 100%. Inhibitory activity was tested 30 min after addition of the compounds. I_{max} indicates maximal inhibition of LPA-induced shape change tested by 5 μM 2CCPA, 3CCPA, octyl thiophosphatidic acid, and NAG and 2 μM octadecenyl phosphate, FPP, and FMP. NE indicates no effect; NS indicates nonsaturated at the highest concentration 5 μM. Values are mean ± S.D. from three different experiments with different platelet donors.

Compounds	Agonist activity		Antagonist activity	
	E_{max}	EC_{50}	I_{max}	IC_{50}
	%	μM	%	μM
Carba-cyclic phosphatidic acid (2CCPA 16:1)	47	NS	35	NS
Carba-cyclic phosphatidic acid (3CCPA 16:1)	48	NS	30	NS
Octyl thiophosphatidic acid	100	2.1 ± 0.5	100	0.74 ± 0.27
Octadecenyl phosphate	100	0.002 ± 0.001	100	0.021 ± 0.01
FPP	100	0.29 ± 0.15	100	0.95 ± 0.3
FMP	100	0.21 ± 0.04	100	0.76 ± 0.35
NAG	NE	NE	NE	NE
H2L 5987411	NE	NE	86	15.5 ± 6.1
H2L 5765834	NE	NE	47	13.73 ± 2.52
AGP 18:1	100	0.0014 ± 0.0003		

LPA-nonresponsive in Ca^{2+} mobilization and CRE-reporter gene assays, whereas CV-1 cells and DRG endogenously express LPA_1 and abundant LPA_7 transcripts (data not shown), suggesting that FPP and NAG could activate other LPA receptors in these cells. Additionally, LPA elevates cAMP in LPA_7-transfected cells (12); therefore, the possibility that simultaneous activation of LPA receptors elevating and decreasing cAMP could modify downstream signals that affect agonist potency.

Oh da *et al.* (22) also reported four residues on LPA_5 that are responsible for the FPP- and NAG-induced receptor activation. Our data confirmed that Arg-276 (Arg-7.32) is a contributing residue in LPA- and FPP-induced receptor activation (Tables 3 and 4). The activation of LPA_5 WT induced by NAG was too weak to examine the effect of the mutants. We identified three additional residues, Arg-2.60, Arg-6.62, and His-4.64, that are critical for ligand recognition in LPA_5. We also generated models of the mutant LPA_5, and we experimentally tested additional hypotheses predicted from these models to further validate the model. The final model resulting from this study serves as an important validated non-EDG family receptor model for phospholipid recognition, and also serves in the future as a template in modeling studies of the other non-EDG family LPA receptors.

In this study, we expanded the pharmacological evaluation of previously identified EDG family LPA receptor-selective agonists and antagonists on LPA_5. These experiments revealed that octyl thiophosphatidic acid and CCPA are selective agonists of LPA_5. To identify novel non-lipid ligands specific for LPA_5, we docked the LPA_5 agonists in the LPA_5 model and developed a receptor-based pharmacophore (Fig. 11). We applied the pharmacophore for *in silico* screening and identified novel non-lipid LPA_5 antagonists (H2L 5987411 and H2L 5765834). These compounds are weak inhibitors with relatively poor efficacy and are nonselective LPA_5 antagonists; however, they provide a valuable starting point for similarity searches and synthetic improvements to optimize the substituent identity and placement on a scaffold already known to provide biological activity. The scaffold defines the overall shape, but differences in electrostatic distribution and localized shape features can produce drastic improvements in potency, efficacy, and selectivity as we have observed in our optimization of LPA_3 receptor antagonists (46).

Although LPA has been considered to be an important mediator of platelet function, the receptor(s) through which LPA stimulates platelets remained unidentified due, in part, to the lack of specific pharmacological tools for probing receptor functions. LPA_5 has been reported to be the most abundantly expressed LPA receptor in human platelets (28, 30, 47). The involvement of LPA_5 in platelet activation because of the lack of understanding its SAR and selective compounds had not been examined. Our data on platelet shape change with LPA_5 agonists and antagonists support the involvement of LPA_5 in LPA-mediated platelet activation. However, the SARs of these compounds on platelets and LPA_5 do not match completely, possibly because of differences in receptor/G-protein coupling

in platelets and heterologous expression systems and/or because of the possible involvement of (an) additional LPA receptor(s) in platelet activation. Interestingly, the dual receptor system for platelet activation has been observed for ADP receptors. Studies using specific agonists suggested that activation of both receptors, P2Y1, coupling to G_q/phospholipase C, and P2Y12, coupling to G_i, is required for a full response of platelets to ADP (48, 49). These observations imply that activation of both G_i- and G_q-mediated pathways might be required to cause platelet aggregation. This study is the first to provide evidence for the involvement of LPA$_5$ in platelet activation. The antagonists that we identified in this study represent a valuable starting point for the identification of more potent LPA$_5$ antagonists in the future. Consequently, understanding the pharmacology of stimulatory and inhibitory LPA receptor(s) in platelets and identifying hits to inhibit these responses will offer novel therapeutic strategies for the prevention and treatment of atherothrombosis.

REFERENCES

1. Tigyi, G. (2001) *Prostaglandins Other Lipid Mediat.* **64,** 47–62
2. Mills, G. B., and Moolenaar, W. H. (2003) *Nat. Rev. Cancer* **3,** 582–591
3. Siess, W., and Tigyi, G. (2004) *J. Cell. Biochem.* **92,** 1086–1094
4. Fang, X., Schummer, M., Mao, M., Yu, S., Tabassam, F. H., Swaby, R., Hasegawa, Y., Tanyi, J. L., LaPushin, R., Eder, A., Jaffe, R., Erickson, J., and Mills, G. B. (2002) *Biochim. Biophys. Acta* **1582,** 257–264
5. Weiner, J. A., and Chun, J. (1999) *Proc. Natl. Acad. Sci. U. S. A.* **96,** 5233–5238
6. Panetti, T. S., Magnusson, M. K., Peyruchaud, O., Zhang, Q., Cooke, M. E., Sakai, T., and Mosher, D. F. (2001) *Prostaglandins* **64,** 93–106
7. Simon, M. F., Chap, H., and Douste-Blazy, L. (1982) *Biochem. Biophys. Res. Commun.* **108,** 1743–1750
8. Rother, E., Brandl, R., Baker, D. L., Goyal, P., Gebhard, H., Tigyi, G., and Siess, W. (2003) *Circulation* **108,** 741–747
9. Kobilka, B. K. (2007) *Biochim. Biophys. Acta* **1768,** 794–807
10. Murakami, M., Shiraishi, A., Tabata, K., and Fujita, N. (2008) *Biochem. Biophys. Res. Commun.* **371,** 707–712
11. Parrill, A. L. (2008) *Biochim. Biophys. Acta* **1781,** 540–546
12. Pasternack, S. M., von Kügelgen, I., Aboud, K. A., Lee, Y. A., Rüschendorf, F., Voss, K., Hillmer, A. M., Molderings, G. J., Franz, T., Ramirez, A., Nürnberg, P., Nöthen, M. M., and Betz, R. C. (2008) *Nat. Genet.* **40,** 329–334
13. Parrill, A. L. (2005) *Biochem. Soc. Trans.* **33,** 1366–1369
14. Valentine, W. J., Fells, J. I., Perygin, D. H., Mujahid, S., Yokoyama, K., Fujiwara, Y., Tsukahara, R., Van Brocklyn, J. R., Parrill, A. L., and Tigyi, G. (2008) *J. Biol. Chem.* **283,** 12175–12187
15. Holdsworth, G., Slocombe, P., Hutchinson, G., and Milligan, G. (2005) *Gene* **350,** 59–63
16. Wang, D. A., Lorincz, Z., Bautista, D. L., Liliom, K., Tigyi, G., and Parrill, A. L. (2001) *J. Biol. Chem.* **276,** 49213–49220
17. Kotarsky, K., Boketoft, A., Bristulf, J., Nilsson, N. E., Norberg, A., Hansson, S., Owman, C., Sillard, R., Leeb-Lundberg, L. M., and Olde, B. (2006) *J. Pharmacol. Exp. Ther.* **318,** 619–628
18. Lee, C. W., Rivera, R., Gardell, S., Dubin, A. E., and Chun, J. (2006) *J. Biol. Chem.* **281,** 23589–23597
19. Tabata, K., Baba, K., Shiraishi, A., Ito, M., and Fujita, N. (2007) *Biochem. Biophys. Res. Commun.* **363,** 861–866
20. Bandoh, K., Aoki, J., Hosono, H., Kobayashi, S., Kobayashi, T., Murakami-Murofushi, K., Tsujimoto, M., Arai, H., and Inoue, K. (1999) *J. Biol. Chem.* **274,** 27776–27785
21. Fujiwara, Y., Sardar, V., Tokumura, A., Baker, D., Murakami-Murofushi, K., Parrill, A., and Tigyi, G. (2005) *J. Biol. Chem.* **280,** 35038–35050
22. Oh da, Y., Yoon, J. M., Moon, M. J., Hwang, J. I., Choe, H., Lee, J. Y., Kim, J. I., Kim, S., Rhim, H., O'Dell, D. K., Walker, J. M., Na, H. S., Lee, M. G., Kwon, H. B., Kim, K., and Seong, J. Y. (2008) *J. Biol. Chem.* **283,** 21054–21064
23. Sardar, V. M., Bautista, D. L., Fischer, D. J., Yokoyama, K., Nusser, N., Virag, T., Wang, D. A., Baker, D. L., Tigyi, G., and Parrill, A. L. (2002) *Biochim. Biophys. Acta* **1582,** 309–317
24. Siess, W., Zangl, K. J., Essler, M., Bauer, M., Brandl, R., Corrinth, C., Bittman, R., Tigyi, G., and Aepfelbacher, M. (1999) *Proc. Natl. Acad. Sci. U. S. A.* **96,** 6931–6936
25. Retzer, M., and Essler, M. (2000) *Cell. Signal.* **12,** 645–648
26. Maschberger, P., Bauer, M., Baumann-Siemons, J., Zangl, K. J., Negrescu, E. V., Reininger, A. J., and Siess, W. (2000) *J. Biol. Chem.* **275,** 19159–19166
27. Haserück, N., Erl, W., Pandey, D., Tigyi, G., Ohlmann, P., Ravanat, C., Gachet, C., and Siess, W. (2004) *Blood* **103,** 2585–2592
28. Khandoga, A. L., Fujiwara, Y., Goyal, P., Pandey, D., Tsukahara, R., Bolen, A., Guo, H., Wilke, N., Liu, J., Valentine, W. J., Durgam, G. G., Miller, D. D., Jiang, G., Prestwich, G. D., Tigyi, G., and Siess, W. (2008) *Platelets* **19,** 415–427
29. Keularts, I. M., van Gorp, R. M., Feijge, M. A., Vuist, W. M., and Heemskerk, J. W. (2000) *J. Biol. Chem.* **275,** 1763–1772
30. Amisten, S., Braun, O. O., Bengtsson, A., and Erlinge, D. (2008) *Thromb. Res.* **122,** 47–57
31. Uchiyama, A., Mukai, M., Fujiwara, Y., Kobayashi, S., Kawai, N., Murofushi, H., Inoue, M., Enoki, S., Tanaka, Y., Niki, T., Kobayashi, T., Tigyi, G., and Murakami-Murofushi, K. (2007) *Biochim. Biophys. Acta* **1771,** 103–112
32. Gerlach, E., and Deuticke, B. (1963) *Biochem. Z.* **337,** 477–479
33. Ballesteros, J. A., and Weinstein, H. (1995) *Methods Neurosci.* **25,** 366–425
34. Halgren, T. A. (1998) *J. Comput. Chem.* **17,** 490–519
35. Baker, D. L., Fujiwara, Y., Pigg, K. R., Tsukahara, R., Kobayashi, S., Murofushi, H., Uchiyama, A., Murakami-Murofushi, K., Koh, E., Bandle, R. W., Byun, H. S., Bittman, R., Fan, D., Murph, M., Mills, G. B., and Tigyi, G. (2006) *J. Biol. Chem.* **281,** 22786–22793
36. Naor, M. M., Walker, M. D., Van Brocklyn, J. R., Tigyi, G., and Parrill, A. L. (2007) *J. Mol. Graph. Model.* **26,** 519–528
37. Bond, S. D., Benedict, J. L., and Laird, B. B. (1999) *J. Comp. Phys.* **151,** 114–134
38. Negrescu, E. V., de Quintana, K. L., and Siess, W. (1995) *J. Biol. Chem.* **270,** 1057–1061
39. Parrill, A. L., Wang, D., Bautista, D. L., Van Brocklyn, J. R., Lorincz, Z., Fischer, D. J., Baker, D. L., Liliom, K., Spiegel, S., and Tigyi, G. (2000) *J. Biol. Chem.* **275,** 39379–39384
40. Inagaki, Y., Pham, T. T., Fujiwara, Y., Kohno, T., Osborne, D. A., Igarashi, Y., Tigyi, G., and Parrill, A. L. (2005) *Biochem. J.* **389,** 187–195
41. Fischer, D. J., Liliom, K., Guo, Z., Nusser, N., Virág, T., Murakami-Murofushi, K., Kobayashi, S., Erickson, J. R., Sun, G., Miller, D. D., and Tigyi, G. (1998) *Mol. Pharmacol.* **54,** 979–988
42. Liliom, K., Tsukahara, T., Tsukahara, R., Zelman-Femiak, M., Swiezewska, E., and Tigyi, G. (2006) *Biochim. Biophys. Acta* **1761,** 1506–1514
43. Durgam, G. G., Tsukahara, R., Makarova, N., Walker, M. D., Fujiwara, Y., Pigg, K. R., Baker, D. L., Sardar, V. M., Parrill, A. L., Tigyi, G., and Miller, D. D. (2006) *Bioorg. Med. Chem. Lett.* **16,** 633–640
44. Szkopińska, A., and Płochocka, D. (2005) *Acta Biochim. Pol.* **52,** 45–55
45. Burstein, S. H., Huang, S. M., Petros, T. J., Rossetti, R. G., Walker, J. M., and Zurier, R. B. (2002) *Biochem. Pharmacol.* **64,** 1147–1150
46. Fells, J. I., Tsukahara, R., Fujiwara, Y., Liu, J., Perygin, D. H., Osborne, D. A., Tigyi, G., and Parrill, A. L. (2008) *Bioorg. Med. Chem.* **16,** 6207–6217
47. Pamuklar, Z., Lee, J. S., Cheng, H. Y., Panchatcharam, M., Steinhubl, S., Morris, A. J., Charnigo, R., and Smyth, S. S. (2008) *Arterioscler. Thromb. Vasc. Biol.* **28,** 555–561
48. Jin, J., and Kunapuli, S. P. (1998) *Proc. Natl. Acad. Sci. U. S. A.* **95,** 8070–8074
49. Pulcinelli, F. M., Ciampa, M. T., Favilla, M., Pignatelli, P., Riondino, S., and Gazzaniga, P. P. (1999) *FEBS Lett.* **460,** 37–40